

Hanna Leitner

# **Cloud formation on tidally locked exoplanets with a G-type host star**

## **BACHELOR'S THESIS**

to achieve the university degree of  
Bachelor's degree programme: Physics

submitted to

**Graz University of Technology**

### **Supervisor**

Prof. Dr.rer.nat. Christiane Helling,  
Institut für Theoretische Physik - Computational Physics

### **Co-Supervisor**

MSc. Sven Kiefer,  
OEAW

## Abstract

To get a better understanding of exoplanets and especially their atmospheres, theoretical models have to be created. The aim of this thesis is to simulate the cloud formation process on tidally locked Hot-Jupiters, which orbit a G-type host star. For this thesis, a new model for creating the General Circulation Model was considered. The radiative transfer happens simultaneously with the material transfer. The new temperature profiles were compared to the older model as in Carone et al. (2020). The cloud formation process was modelled for planets with equilibrium temperatures ranging from 2600 K to 1200 K in 200 K steps. For each planet, two mixing models were considered and simulated. Information about the nucleation process, the bulk growth and the cloud distribution were obtained, as well as data about the number of particles and the element composition. Visualisations in form of plots were created to get a better idea of the processes in the planet's atmosphere. The findings of this project suggest that planets with a lower equilibrium temperature have a more prominent nucleation formation rate, more bulk growth and therefore have more cloud particles. Planets with higher equilibrium temperature have clouds predominately on the night side, with lower equilibrium temperatures the clouds exist all around the planet. Overall, this thesis provides an overview of the considered planets and the cloud formation process in their atmospheres. The collected data could be of use for future projects, which calculate the clouds inside the GCM, as the simulations offer an understanding about the calculations of the cloud formation process in different planetary atmospheres.

# Contents

|          |  |           |
|----------|--|-----------|
| <b>1</b> | <b>Introduction</b>                                  | <b>2</b>  |
| 1.1      | Comparison of models . . . . .                       | 2         |
| 1.2      | Cloud formation process . . . . .                    | 3         |
| 1.3      | Motivation . . . . .                                 | 6         |
| <b>2</b> | <b>Methods</b>                                       | <b>7</b>  |
| 2.1      | General Circulation Model . . . . .                  | 7         |
| 2.2      | Cloud formation simulations . . . . .                | 8         |
| 2.3      | Comparing models . . . . .                           | 9         |
| <b>3</b> | <b>Results</b>                                       | <b>10</b> |
| 3.1      | Cloud Model Results . . . . .                        | 10        |
| 3.1.1    | 2600 K equilibrium temperature . . . . .             | 11        |
| 3.1.2    | 1600 K equilibrium temperature . . . . .             | 20        |
| 3.1.3    | Planets with other equilibrium temperature . . . . . | 28        |
| 3.2      | Comparison to older models . . . . .                 | 30        |
| <b>4</b> | <b>Discussion</b>                                    | <b>31</b> |
| <b>5</b> | <b>Conclusion</b>                                    | <b>34</b> |

# Chapter 1

## Introduction

As of now, there are 5863 confirmed exoplanets<sup>1</sup>. With this many planets and yet more to find, the question arises how these planets function or what kind of environment they exhibit. To understand the composition and physical and chemical processes on the exoplanets, models have to be created. One of these processes is the formation of clouds in these exoplanetary atmospheres. These formation processes are diverse and depend on the element composition, the temperature, the distance to its host star and their orbiting period as well as other factors.

For the purpose of this study the cloud formation process of Jupiter similar planets was studied. The planets are tidally locked and are considered Hot-Jupiters. The planets have a gravitational acceleration of  $1000 \text{ ms}^{-2}$  and orbit a G-type host star. This host star has an effective temperature of 5660 K.

### 1.1 Comparison of models

For the purpose of this bachelor thesis, a new model has been considered. The simulations of the cloud formation on different exoplanets have already been done; for reference see Helling et al. (2023). The previous model used an idealized radiative heating approach in a 3D General Circulation Model. The pressure-temperature profile and the radiative time scales were based on the stellar irradiation angle. The 3D GCM uses this data and puts it in per material transport step. During the process Newtonian Cooling is considered, which means that the rate of the heat loss in the atmosphere is directly proportional to the temperature difference between the atmosphere and its environment. Disadvantages of this approach include the night

---

<sup>1</sup><https://exoplanet.eu/home/> accessed 10.06.2024

side getting too cool and the radiative heating and the material transfer not being at the same time. This model was used in Carone et al. (2020).

Using a new approach, the new model now includes the full radiative transfer calculation inside the 3D GCM. This means, the stellar irradiation is calculated coupled with the material transport. The 3D GCM now calculates each profile with the coupling of the transport of the gas and the interaction with radiation. The temperature of the gas phase is of higher accuracy in this model as well. Having this extra step leads to more computing time and a more complex understanding of the radiative transfer. Here, the radiative transfer on the night side has to be compared to the day side considering the strong wind jet. A thing that is not yet considered, is the cloud impact on the 3D GCM, as here the clouds are simulated with a finished GCM. This model was taken from Schneider et al. (2022).

## 1.2 Cloud formation process

In contrast to the earths water clouds, exoplanets exhibit a rich chemical diversity as there are many different chemical compounds present (Helling, 2019). The process of cloud formation is depicted in a diagram in figure 1.1.

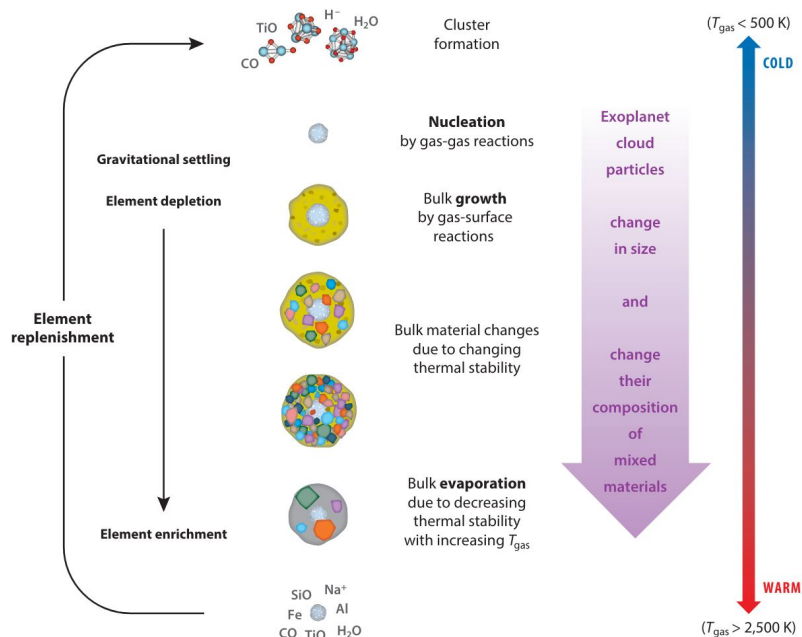


Figure 1.1: Cloud formation process in exoplanet atmospheres, image taken from Helling (2019).

On gas giants there are cloud particles in the form of silicates, metal oxides and more (Helling, 2019). For clouds to form there need to be nuclei or condensation seeds. If there are no nuclei present, coming from volcanic dust or meteorites for example, they need to form from the gas phase (Helling, 2021). The formation of the nuclei depends on the present elements as well as the thermodynamic conditions (Helling, 2021). Gas-gas reactions start the process, whereby molecular clusters can form with varying sizes and complexities. This results in a change from the gas phase to the solid phase and the creation of cloud condensation nuclei. These offer the first surface which enables bulk growth (Helling, 2022). This means thermally stable elements may now condensate onto the existing nuclei. The particles are able to gain mass and size and start falling through the atmosphere. This is due to gravitational settling, which is dependent on the gravitational force as well as the frictional force on the particles (Helling, 2022). Different layers of the atmosphere show different thermodynamic conditions, which bring forth different composition of the cloud particles (Helling, 2019). Elements become stable and grow onto the cloud particle and it grows further. It is also possible that the change in thermodynamic conditions causes elements to become unstable and evaporate, which results in shrinkage (Helling, 2022). The growth of the particles continues until the temperature reaches too high values and the particles evaporate (Helling, 2019). To keep the cloud formation process active, the particles need to be moved again after evaporation. This can happen by diffusion or convective mixing, which leads to the elements being transported through the atmosphere (Helling, 2019). This so called element replenishment keeps the element depletion in the upper layers and the element enrichment in the lower parts in balance (Helling, 2019). Photochemistry is also an important factor that has impact on the element composition of the atmosphere as in Baeyens et al. (2022).

The nucleation species  $\text{TiO}_2$  and  $\text{SiO}$  can be found in the highest layer of the atmosphere. The middle part of the cloud layer consists of a diverse mix of  $\text{Mg}/\text{Fe}/\text{Si}/\text{O}$  and other materials containing  $\text{Ca}$  and  $\text{Al}$ . The hottest area of the clouds consists of condensates like  $\text{Fe}[\text{s}]$ ,  $\text{Al}_2\text{O}_3[\text{s}]$ ,  $\text{CaTiO}_3[\text{s}]$  (Helling, 2022).

Planets can be differentiated based on their global temperature. Here, the equilibrium temperature  $T_{eq}$  was used. This property is defined as having a planet with equal bond albedo and semi-major axis as an isothermal sphere. It can be calculated using the stellar temperature  $T_*$ , the stellar radius  $R_*$ , the planets semi major axis  $d$  and the bond albedo of the planet  $\alpha_B$ . The bond albedo, so how much of the light is scattered back from the planet to space, was set to zero in the course of this thesis. The heat distribution factor  $f$  which is multiplied to the equilibrium temperature was chosen as  $\frac{1}{4}$ . This was chosen under the assumption that heat distribution is efficient. Using this factor, one would get the day side brightness temperature, here

the definition is used for the equilibrium temperature.

$$T_{eq} = T_* \sqrt{\frac{R^*}{2d}} (f(1 - \alpha_B))^{\frac{1}{4}} \quad (1.1)$$

Information regarding the equilibrium temperature has been taken from Koll (2022).

In the planetary atmosphere, there are jets which are responsible for material transport inside the atmosphere. The wind velocities get greater for planets with a higher equilibrium temperature (Baeyens et al., 2021). The jet shifts the gas in an anticlockwise manner for planets with anticlockwise rotation. The gas gets transported over the morning terminator (Baeyens et al., 2021). For shorter rotation periods, so the planets with a higher equilibrium temperature, the planets show deeper equatorial jets (Schneider et al., 2022) (Baeyens et al., 2021). The hot gas transported by the jet and the hotter regions get not only pushed on the equator but also to different latitudes. This leads to there being hotter regions as well (Baeyens et al., 2021). Having these areas of hotter regions has a direct impact on the cloud formation process.

Another important factor for the cloud formation process is the mixing rate. The planets climate is linked to the winds and the chemistry (Baeyens et al., 2021). This gives information on how effectively the particles are moved to the upper atmosphere again after evaporation. For the purpose of this bachelor thesis, two cases were considered. Normal mixing describes the efficient process of element replenishment. Due to observations the reduced mixing was introduced, which reduces the mixing speed (Samra et al., 2023). For this thesis, this scaled mixing is less efficient and was scaled with a factor of 100. The mixing time scale  $\tau_{mix}$  gives information on how fast the material are brought up again. This uses the velocity  $v$  of how fast the particles move up and down and the height  $z$  of the atmosphere.

$$\tau_{mix}(z) = \int_0^z \frac{1}{v(z')} dz' \quad (1.2)$$

The formula and its explanation can be found in Helling et al. (2023).

## 1.3 Motivation

The purpose of this Bachelor thesis is to simulate and study cloud formation in exo-planetary atmospheres based on results from a new 3D GCM which gives information about the local temperature, pressure and the velocity field of the atmosphere. In the previous model a simplified version was considered. It is important to have models that can explain the cloud formation process to be able to compare and interpret observations of real planets.

The data from the General Circulation Model was used to create cloud simulations for different exoplanets orbiting G-type stars. With the data the cloud formation process was simulated. The goal of the thesis is to get a better understanding of the clouds in these exoplanet atmospheres. Planets with different equilibrium temperatures and mixing efficiencies were considered. Both factors have direct impact on the cloud formation process. The temperature influences where clouds can form and what area of the planet is covered and also at which point they evaporate. The mixing shows how efficient the element replenishment is and has then impact on the nucleation rate, the bulk growth and the cloud distribution.

# Chapter 2

## Methods

In the following sections, the methods used over the course of this project will be focusing on what data has been created and how the cloud formation process was simulated. The outcome and observations of the simulations will be commented on in the results 3. In the discussion 4 part of this thesis the connection between the individual factors will be drawn.

### 2.1 General Circulation Model

In order to simulate the cloud formation process, first a General Circulation Model (GCM) was created. Over 1000 simulation days the processes in the planet's atmosphere were simulated. This data has been created by Dr. Ludmila Carone and has been provided. This data included information about local pressure, gas temperature, winds and the corresponding height at different layers of the atmosphere.

Using the created data, the cloud simulations could be made. Hereby the "Static Weather" code was provided, which was created by Prof. Christiane Helling and Dr. Peter Woitke. More information to this theoretical background can be found in Woitke and Helling (2003), Woitke and Helling (2004), Helling et al. (2004), Helling et al. (2008). The cloud formation process could then be modeled. The simulations gave information about the nucleation, the bulk growth and the cloud distribution. Furthermore, the particle number densities at each layer and number densities of ions, atoms and molecules can be ascertained.

## 2.2 Cloud formation simulations

The formation of clouds was looked at for various planets with different global parameters. For all planets, the effective temperature of the host star was set to  $T_{eff} = 5660$  K. The gravitational acceleration was  $1000 \text{ ms}^{-2}$  for all planets. For each planet, the cloud formation process was simulated for the normal and scaled mixing model. The equilibrium temperature of the planets itself ranged from 2600 K to 1200 K for normal mixing. At the point of writing this thesis, the scaled mixing profiles of 1400 K and 1200 K were not finished yet, but they have been run later. This means, for scaled mixing there are results between 2600 K and 1600 K included. The range of the equilibrium temperature was taken in 200 K steps. The planet's atmospheres were modeled after creating a 3D GCM for the planet. Profiles were created for the longitudes of  $-150^\circ$ ,  $-120^\circ$ ,  $-90^\circ$ ,  $-60^\circ$ ,  $-30^\circ$ ,  $0^\circ$ ,  $30^\circ$ ,  $60^\circ$ ,  $90^\circ$ ,  $120^\circ$ ,  $150^\circ$  and  $180^\circ$  and latitudes of  $0^\circ$ ,  $23^\circ$ ,  $45^\circ$  and  $68^\circ$ . For later visualisations of the results, the upper hemisphere was mirrored for the southern hemisphere. Using these points gives 48 profiles for the planet. The calculations started at  $10^{-5}$  bar in the highest layer and reached 650 bar in the deeper atmosphere. For certain profiles, the simulations did not reach 650 bar; therefore, some were rerun with either a longer runtime or an adapted tolerance for the numerical solver.

The resulting data gives information about the cloud formation process in the atmospheres. To be more precise, there is information about where nucleation happens and how the particles grow as they reach deeper layers. The number of particles in the individual layers and the element composition of them can be determined. The individual profiles were taken and interpolated to create a picture of the whole atmosphere.

The plots were created for all planets shown from two sides. For the equatorial slice the planet is cut in half at the equator and looked at from above. The perspective has a latitude of  $0^\circ$  everywhere. At  $0^\circ$  longitude, the sub stellar point is located. This point is on the day side facing the host star directly. The anti stellar point is at  $180^\circ$  on the night side, permanently facing away from the star. The evening terminator is at  $90^\circ$ . The morning terminator is at  $-90^\circ$ , however, in the course of this thesis,  $270^\circ$  is also used which is to be looked at as an equal point.

The other perspective is from the terminator slice, which cuts the planet in half from top to bottom. The planet is in between the host star and the viewer. Here, the different latitudes are shown. The longitudes are  $90^\circ$  and  $-90^\circ$ , with the evening terminator on the west side and the morning terminator on the east side. The pressure is plotted logarithmically for all plots. To get a better look at the atmosphere, it was stretched, the inner white circles represent the inner part of the planet, but are not accurate in size. The scales were chosen appropriately to be able to compare the

planets with each other, but still be able to observe the individual features of each planet.

For all planets, the gas temperature distribution  $T_{gas}$  [K] was visualised. Hereby, there was no difference for normal and scaled mixing. This is due to the GCM being created without the clouds in it. This means, the impact of the clouds on the temperature has not been considered. The cloud formation was visualised with three different parts of the process. Starting with where the clouds are located in the atmosphere. This was done using the dust to gas ratio  $(\rho_{dust}/\rho_{gas}) \cdot 10^{-3}$ , where a higher ratio is related to higher ratio of mass densities in that region. An important stage is the nucleation phase. To enable nucleation, the temperature has to be sufficiently low. The higher the total nucleation rate  $J_*$  [ $\text{cm}^{-3}\text{s}^{-1}$ ], the more nuclei can be generated in that area. As the particles fall through the atmosphere they start growing. To get an idea of the size of them, the mean particle size  $\langle a \rangle$  [ $\mu\text{m}$ ] is depicted. This shows how the particles grow throughout the atmosphere and also where the particles cease to exist.

To get a more detailed perspective, more plots have been created. The plotting routine was adjusted by Tamara Janz who then also created the plots. Here the profile at the morning terminator for both scaled and normal mixing is shown. The gas temperature and the mixing time scales can be observed in the plots. To get a better understanding of the the dust to gas ratio, nucleation process, the particle growth and the number of the particles, plots for these factors were created as well. They are depicted in the order of temperature and mixing time scales, dust to gas ratio, nucleation rate, mean particle size and particle number in figures 3.2, 3.5, 3.8, 3.11, 3.12 for  $T_{eq} = 2600$  K. This was repeated for  $T_{eq} = 1600$  K in figures 3.14, 3.17, 3.20, 3.23, 3.24. Here, it is especially interesting to observe the relationship between these factors and how they impact the cloud formation process.

## 2.3 Comparing models

In the course of this project, a new cloud formation model was simulated based on the new 3D GCM. While creating the data, differences between the gas temperature between the older model and the newer model were noticed. To visualise this difference, a Python code that takes the input of the data from the old model and the new model, was created. Using the data, the temperature progress throughout the atmosphere was plotted for the day side  $0^\circ$ , the evening terminator  $90^\circ$ , the night side  $180^\circ$  and the morning terminator  $-90^\circ$ , the latitude was kept constant at  $0^\circ$ . With this the difference of the temperature profiles could be evaluated. The profiles for all planets can be observed in the appendix 5 in figure 5.8, the planet with 2600 K equilibrium temperature is described in more detail in results 3 in figure 3.26.

# **Chapter 3**

## **Results**

As described in chapter 2, the GCM was run over 1000 simulation days in an exoplanet atmosphere. Using this data, simulations of cloud formation were made. The data files give a deeper understanding of how the process starts, namely where nucleation happens and what elements can be found at what point in the atmospheres. The mean size of the cloud particles can also be looked at, as well as where the clouds will exist.

### **3.1 Cloud Model Results**

In the following section, the observations of two considered exoplanets will be described in detail. Namely, the planets with an equilibrium temperature of 2600 K and 1600 K have been chosen as they show major differences regarding the clouds. The visualisations of the other planets can be found in the appendix 5 and will be commented on at the end of this section.

### 3.1.1 2600 K equilibrium temperature

#### Gas temperature distribution

In figure 3.1 the gas temperature distribution of a planet with 2600 K equilibrium temperature is depicted. As this data has been taken directly from the GCM, the effect of clouds on the atmosphere has not been considered, therefore there is no difference between normal and scaled mixing. In subfigure 3.1i, the equatorial slice of the planet is shown, in subfigure 3.1ii the terminator slice.

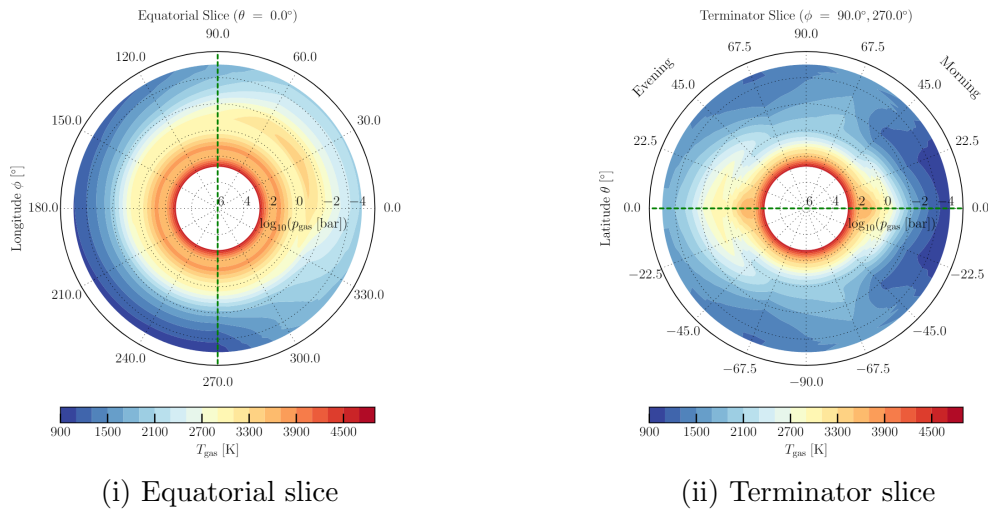


Figure 3.1: Gas temperature distribution in K on a tidally locked planet with an equilibrium temperature of 2600 K with a a G-type host star with  $T_{\text{eff}} = 5660$  K.

Focusing on the lower part of the atmosphere, where the pressures rises above 100 bar the temperature is evenly distributed around the planet and reaches up to 4700 K. As the pressure falls in the upper part of the atmosphere the temperature falls as well. In the atmosphere's layer where the pressure is below  $10^{-4}$  bar the gas temperature is not evenly distributed. On the day side the temperature reaches about 2100 K. On the night side and at the morning terminator at  $270^\circ$  the temperature sinks to its lowest point of 900 K in the upper atmosphere. Around  $30^\circ$  there is a point in the atmosphere between 1 bar and 0.01 bar, where the temperature rises again before falling further. Looking at the terminator slice in subfigure 3.1ii the gas temperature on the morning side sinks to 900 K in the region between  $22^\circ$  and  $-22^\circ$  in the upper layers. In contrast to this, on the evening side the temperature is at about 2000 K in this area. At the  $68^\circ$  and  $-68^\circ$  mark on the evening side the temperature reaches 1200 K, and on the morning side this area is warmer reaching 2000 K in the upper layer. The inner atmosphere is evenly distributed at about 4700 K.

In figure 3.2 the gas temperature at the morning terminator is depicted. The mixing time scales are included as well.

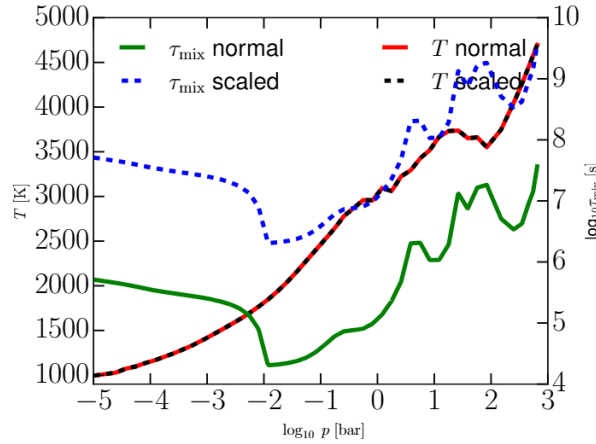


Figure 3.2: Gas temperature at the morning terminator for more (red) and less (black) efficient mixing, mixing time scales for more (green) and less (blue) efficient mixing, created by Tamara Janz.

The temperature specifically at the morning terminator for the more and less efficient mixing model are equal as the clouds impact has not been considered. The temperature rises at lower layers of the atmosphere, meaning at higher pressures. This rise is mostly steady, at around 1 bar the temperature sinks before rising again. The temperature at  $10^{-5}$  bar is at 900 K. At 650 bar the temperature reaches its maximum of 4700 K. The temperature profile can be compared to figure 3.1. Looking at the morning terminator there, the findings are consistent with the profile here.

Looking at mixing time scales, there are differences notable for the scaled and normal mixing scenario. After decreasing steadily both profiles drop at  $10^{-2}$  bar. Between 1 bar and 10 bar the mixing keeps getting slower and faster again. Both profiles have their maxima and minima at the same layers of the atmosphere. For scaled mixing the peak reaches between  $10^9$  s and  $10^{10}$  s at 650 bar. The normal mixing model has its peaks between  $10^7$  s and  $10^8$  s at 650 bar.

### Dust to gas ratio

In figure 3.3, the dust to gas ratio is visible for a planet with an equilibrium temperature of 2600 K. In this case, the simulation was made using the normal mixing model. In the left subfigure 3.3i, the equatorial slice is depicted, in the right subfigure 3.3ii, the terminator slice. In figure 3.4, the dust to gas ratio for the scaled mixing model is depicted. In subfigure 3.4i, the equatorial slice can be observed, in subfigure 3.4ii, the terminator slice.

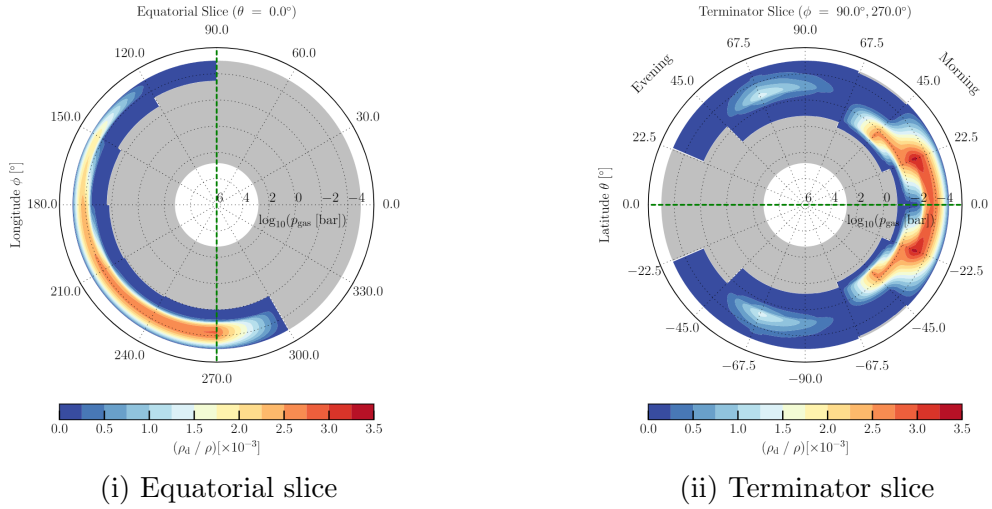


Figure 3.3: Gas to dust ratio distribution scaled with  $10^{-3}$  on a planet with an equilibrium temperature of 2600 K with normal mixing.

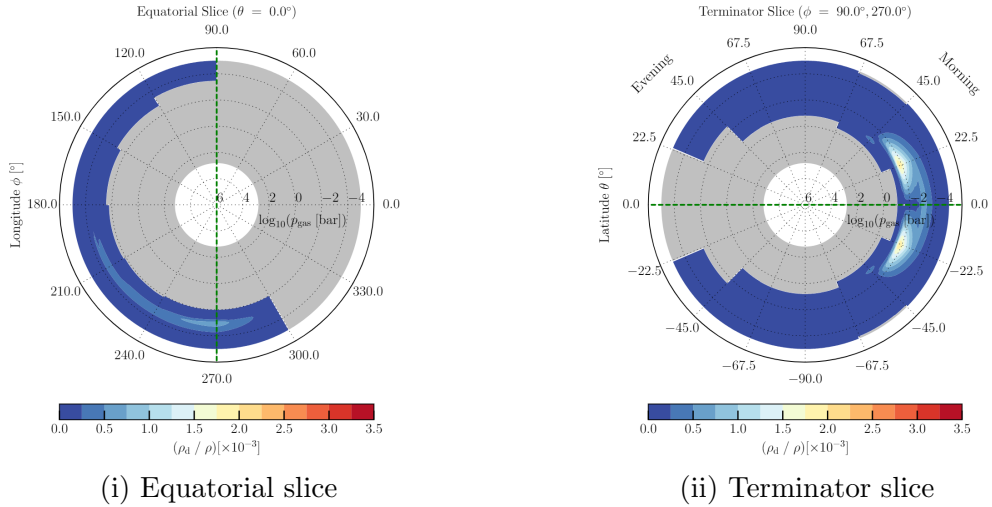


Figure 3.4: Dust to gas ratio distribution scaled with  $10^{-3}$  on a planet with an equilibrium temperature of 2600 K with scaled mixing.

For the equatorial slice in figure 3.3i the clouds reach from the evening terminator at  $90^\circ$  over the morning terminator to  $330^\circ$  on the day side where they shift over. The highest ratio is located around the  $10^{-4}$  bar mark and reaches  $2.5 \cdot 10^{-3}$ . At 0.01 bar the clouds cut off and cease to exist in the lower atmosphere. For the terminator slice the ratio has its peak at the  $22^\circ$  and the  $-22^\circ$  mark on the morning side of the planet, reaching up to  $3.5 \cdot 10^{-3}$ . The clouds stretch from the evening side at  $22^\circ$  over the morning side and back to  $-22^\circ$  on the evening side. The highest value on the evening side is at  $68^\circ$  and  $-68^\circ$  with  $1 \cdot 10^{-3}$ . At  $45^\circ$  and  $-45^\circ$  on the morning side the clouds reach their deepest point into the atmosphere.

In subfigure 3.4i the clouds reach from the evening terminator at  $90^\circ$  over the morning terminator up to  $330^\circ$ . The peak of the ratio is between 0.01 bar and  $10^{-4}$  bar and reaches around  $1 \cdot 10^{-3}$  as its peak on the morning terminator. The clouds do not reach further than 0.01 bar into the atmosphere. At the terminator slice, one can see a peak of the ratio at  $22^\circ$  and  $-22^\circ$  on the morning side. The ratio reaches up to  $2 \cdot 10^{-3}$  there. The clouds are distributed around the planet from  $22^\circ$  on the evening side to  $-22^\circ$  on the evening side. At  $68^\circ$  on the evening side there is a little peak visible at 0.01 bar. The clouds reach at  $45^\circ$  and  $-45^\circ$  to nearly 1 bar at their lowest point.

In figure 3.5 the dust to gas ratio for the morning terminator is depicted.

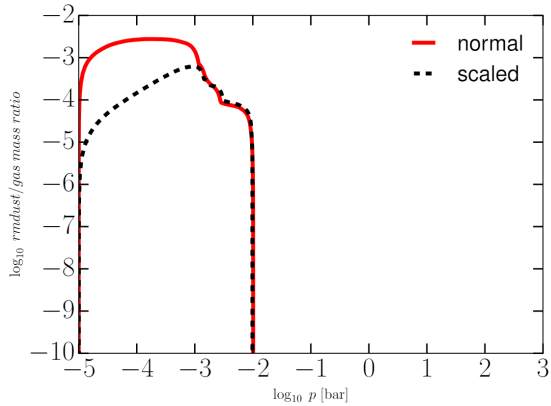


Figure 3.5: Dust to gas ratio for normal (red) and scaled (black) mixing at the morning terminator, created by Tamara Janz.

At  $10^{-5}$  the ratio appears as here the first clouds are simulated. For the normal mixing model the ratio reaches a constant value of around  $2.5 \cdot 10^{-3}$ . Getting into deeper layers, the ratio starts dropping and goes towards 0 at  $10^{-2}$  bar. The scaled mixing shows consistent growth between  $10^{-5}$  bar and  $10^{-3}$  bar. At higher pressures it starts dropping and plummets to 0 at  $10^{-2}$  bar.

### Total nucleation rate

In figure 3.6 the total rate of nucleation can be seen for a planet with an equilibrium temperature of 2600 K for the normal mixing scheme. Subfigure 3.6i shows the scenario from the equatorial side. The terminator side is to be seen in subfigure 3.6ii. Figure 3.7 depicts the total nucleation rate for the planet with scaled mixing. Subfigure 3.7i shows the equatorial and subfigure 3.7ii the terminator slice.

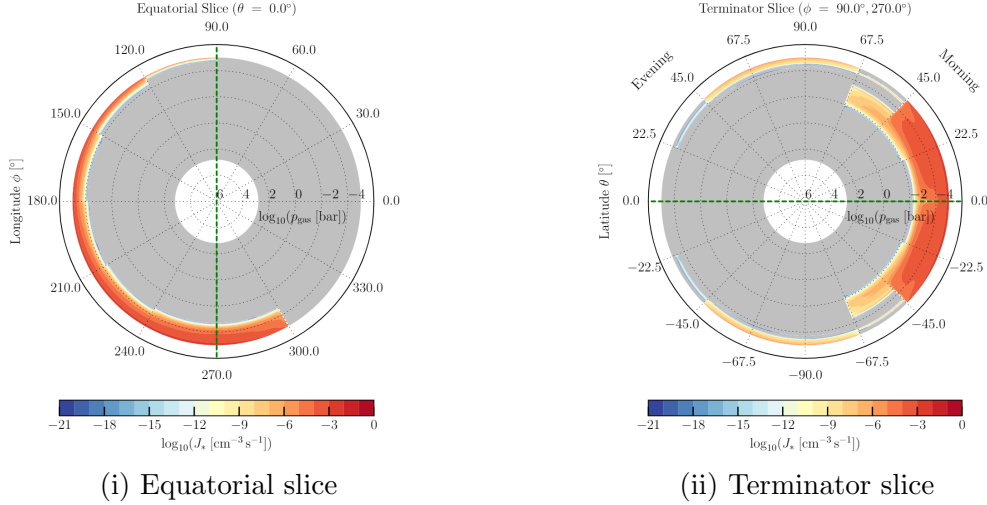


Figure 3.6: Total nucleation rate on a planet with an equilibrium temperature of 2600 K with normal mixing.

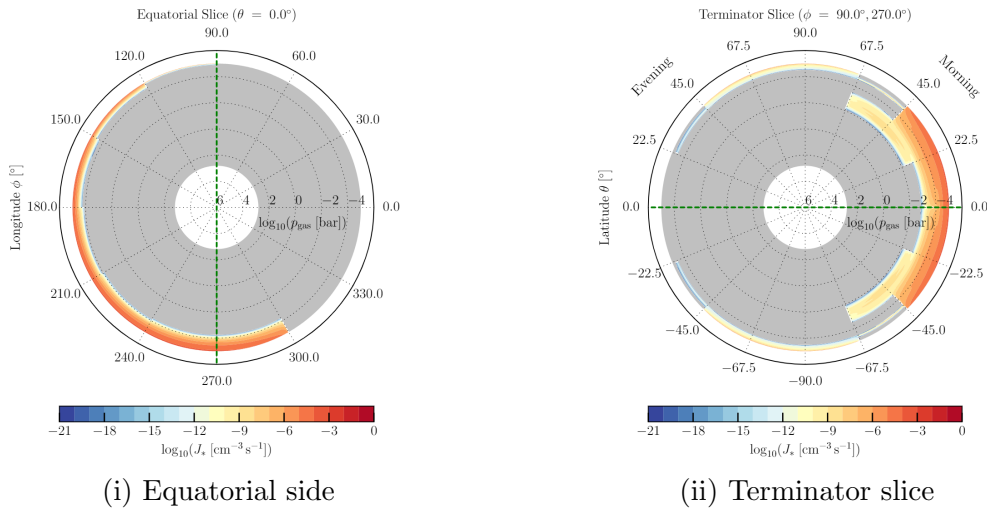


Figure 3.7: Total nucleation rate on a planet with an equilibrium temperature of 2600 K with scaled mixing.

Looking at the equatorial slice in figure 3.6i, one can see that nucleation is possible down to over  $10^{-4}$  bar in the atmosphere. At its highest value, it reaches  $0.1 \text{ cm}^{-3}\text{s}^{-1}$  and at its lowest, around  $10^{-20} \text{ cm}^{-3}\text{s}^{-1}$ . At the terminator slice, the nucleation is dominant on the morning side especially from  $0^\circ$  to  $45^\circ$  and  $-45^\circ$ . From  $45^\circ$  to  $68^\circ$  nucleation is not possible in the highest layer and rather between  $10^{-4}$  bar and  $10^{-2}$  bar. From  $22^\circ$  and  $-22^\circ$  on the evening side to  $68^\circ$  and  $-68^\circ$  degrees on the morning side, nucleation is possible only in the upmost region of the atmosphere down to  $10^{-4}$  bar. The equatorial slice in figure 3.7i shows nucleation in the upper atmosphere down to  $10^{-4}$  bar, from values of  $0.1 \text{ cm}^{-3}\text{s}^{-1}$  to around  $10^{-20} \text{ cm}^{-3}\text{s}^{-1}$ . Nucleation is possible on the night side starting at  $120^\circ$  and over the morning terminator to  $300^\circ$ . The equatorial slice shows nucleation on the morning side from  $-45^\circ$  to  $45^\circ$  as its highest value. From  $22^\circ$  and  $-22^\circ$  to  $68^\circ$  and  $-68^\circ$  nucleation is not possible in the upmost region but rather between  $10^{-4}$  bar to  $10^{-2}$  bar. Starting at  $68^\circ$  and  $-68^\circ$  on the morning side to  $22$  and  $-22^\circ$  on the evening side nucleation is possible in the highest layer of the atmosphere down to  $10^{-4}$  bar.

In figure 3.8 the total nucleation rate is shown. The profile here is specifically for the morning terminator to get a more detailed view there using the normal and scaled mixing model.

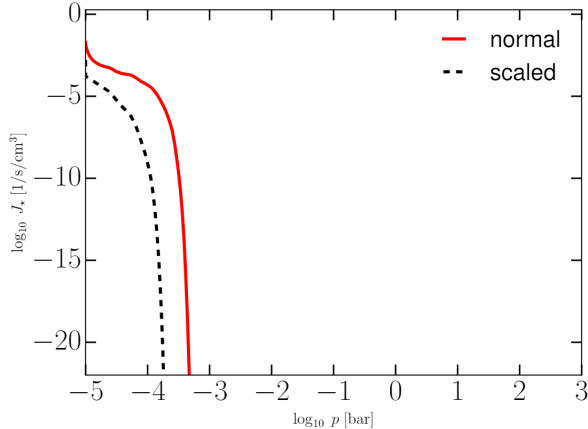


Figure 3.8: Total nucleation rate at the morning terminator for normal (red) and scaled (black) mixing, created by Tamara Janz.

The total nucleation rate is the highest at  $10^{-5}$  bar. Here, the total nucleation rate has a value of  $0.1 \text{ cm}^{-3}\text{s}^{-1}$  for the normal mixing. In the deeper layers, the nucleation rate sinks and reaches 0 between  $10^{-4}$  and  $10^{-3}$ . The scaled mixing model starts at lower value. The total nucleation rate does not reach as far into the atmosphere as the normal mixing profile.

### Mean particle size

In figure 3.9 the mean particle size can be seen for a planet with an equilibrium temperature of 2600 K and the normal mixing model. In subfigure 3.9i the mean particle size on the equatorial slice is visible. In subfigure 3.9ii, it can be observed from the terminator slice. In figure 3.10 the planet with scaled mixing is depicted. In subfigure 3.10i the planet is looked at at the equatorial slice, and subfigure 3.10ii at the terminator slice.

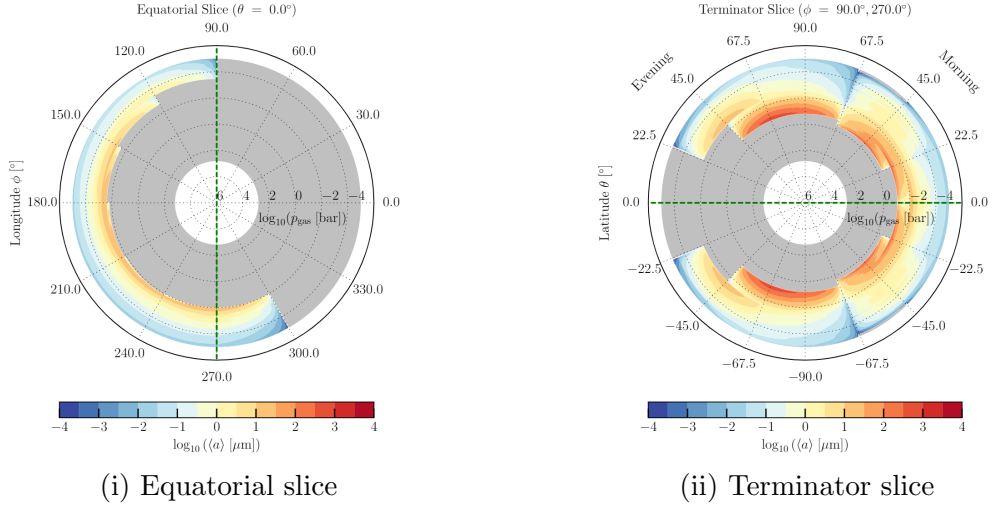


Figure 3.9: Mean particle size distribution on a planet with an equilibrium temperature of 2600 K with normal mixing.

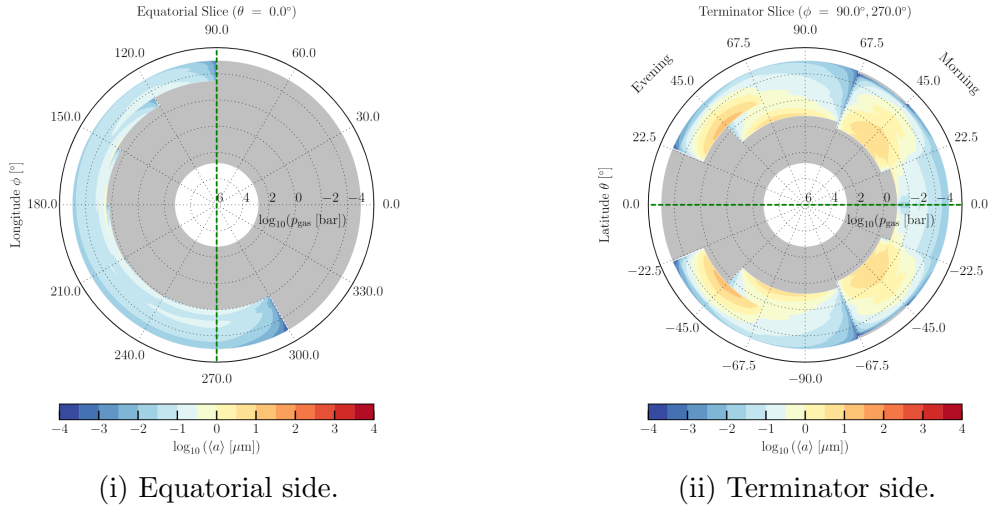


Figure 3.10: Mean particle size distribution on a planet with an equilibrium temperature of 2600 K with scaled mixing.

The mean particle size shows not only how big the particles are at certain parts in the atmosphere but also the location of the cloud particles. Therefore, the extent of the mean particles size is equal to the area of the cloud distribution in figure 3.3. The biggest particles for normal mixing in figure 3.9 at  $10 \mu\text{m}$  are found at 0.01 bar, before they cut off. In lower parts of the atmosphere, there are no cloud particles to be found. Looking at it from the terminator slice perspective, the cloud particles reach about 1 bar deep where they are at their biggest at  $1000 \mu\text{m}$ .

The mean particle size is depicted for the same area as the dust to gas ratio in figure 3.4. Looking at the equatorial side for scaled mixing the particles reach 0.01 bar into the atmosphere and grow up to  $0.1 \mu\text{m}$ . For the terminator slice, particles reach down to nearly 1 bar at  $45^\circ$  on the morning side. The particles are at their biggest  $10 \mu\text{m}$  in size which happens at  $45^\circ$  and  $-45^\circ$  at around 1 bar on the morning side. Considering the evening side the peak is at  $45^\circ$  and  $-45^\circ$  at around  $10^{-2}$  bar.

In figure 3.11 the mean particles size at the morning terminator can be seen.

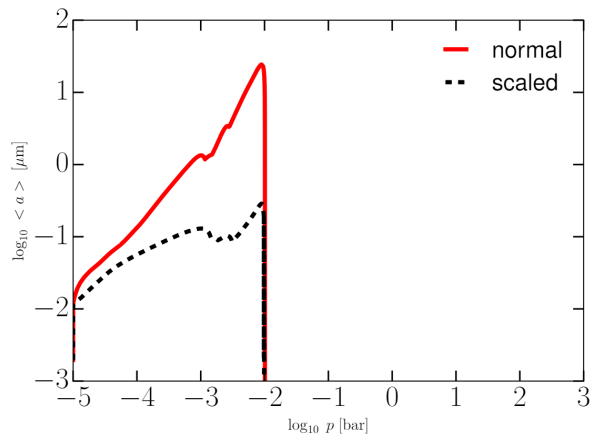


Figure 3.11: Mean particle size at the morning side for normal (red) and scaled (black) mixing, created by Tamara Janz.

The mean particle size at the morning terminator shows growth between  $10^{-5}$  bar and  $10^{-2}$  bar. The normal mixing profile has its peak between  $10 \mu\text{m}$  and  $100 \mu\text{m}$ . At  $10^{-3}$  bar there is small drop in the size. The scaled mixing has its peak between  $0.1$  and  $1 \mu\text{m}$ . Between  $10^{-3}$  bar and  $10^{-2}$  bar the size gets smaller before growing again. For both profiles the particle size reaches 0 at  $10^{-2}$  bar where the particles cease to exist.

### Number of particles

In figure 3.12 the number of particles in the atmosphere is visible. The profiles are created for normal and scaled mixing respectively.

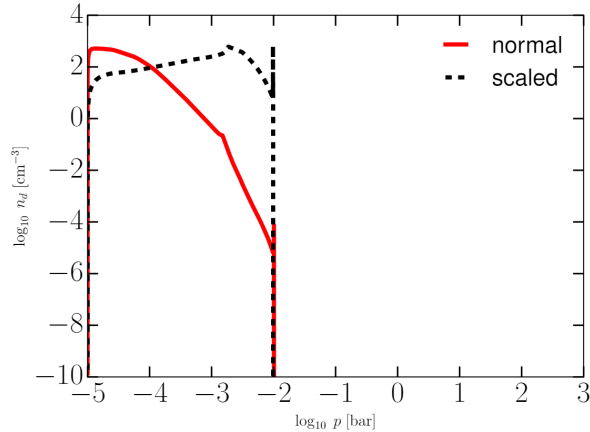


Figure 3.12: Number of particles on the morning terminator for normal (red) and scaled (black) mixing, created by Tamara Janz.

In the highest layer where nucleation is possible, the normal mixing profile has a higher number of particles. At  $10^{-4}$  bar, both profiles show an equal number of particles of  $10^2 \text{ cm}^{-3}$ . In the deeper layers, the scaled mixing profiles has a higher value and reaches its peak between  $10^{-3}$  bar and  $10^{-2}$  bar. At  $10^{-2}$  bar, both profiles approach 0 rapidly.

### 3.1.2 1600 K equilibrium temperature

#### Gas temperature distribution

The temperature distribution for a planet with an equilibrium temperature of 1600 K is depicted in figure 3.13. In subfigure 3.13i the planet is visible on the equatorial slice. The terminator slice can be observed in subfigure 3.13ii. Here, there is no difference for normal and scaled mixing.

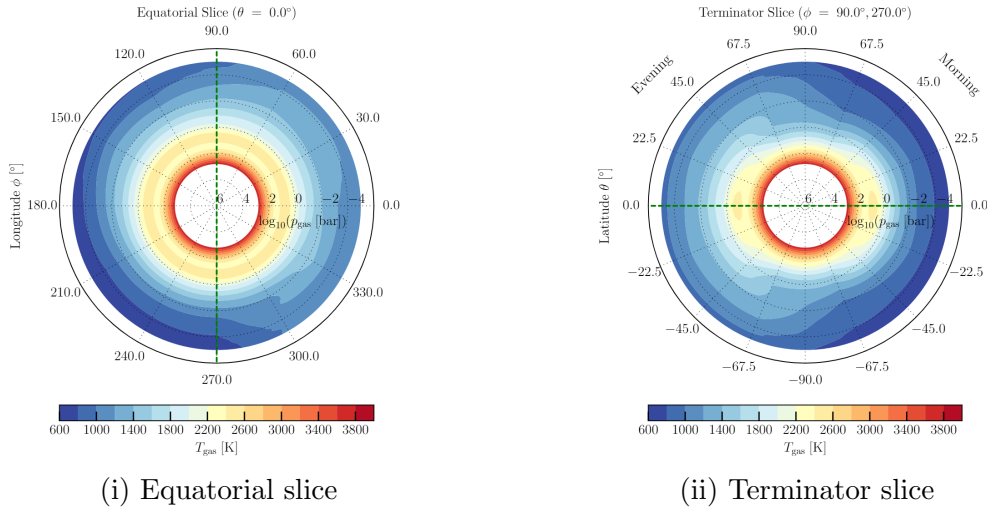


Figure 3.13: Gas temperature distribution on a tidally locked planet with an equilibrium temperature of 1600 K with a G-type host star with  $T_{\text{eff}} = 5660$  K.

The temperature on the equatorial slice is equally distributed in the lower part of the atmosphere reaching up to 4200 K. For the upper part of the atmosphere, the temperature shows differences for the night and day side. In the upmost part, the temperature sinks to 900 K on the night and shifts over the morning terminator. On the morning side the highest temperature in the highest atmosphere layer at  $10^{-4}$  bar can be found at  $30^\circ$ . For the terminator slice the temperature is overall lower on the morning side reaching down to 900 K between  $68^\circ$  and  $-68^\circ$ . On the evening side the temperature is at around 1100 K in the top layer of the atmosphere. In the deepest part, the temperature is around 4200 K around the planet. When looking at the  $0^\circ$  mark at either side, one notices a spot where the temperature rises briefly before sinking again between 1 bar and 100 bar.

In subfigure 3.14 the temperature profile at the morning terminator is visible. The mixing time scales are visible as well. This is depicted for scaled and normal mixing receptively.

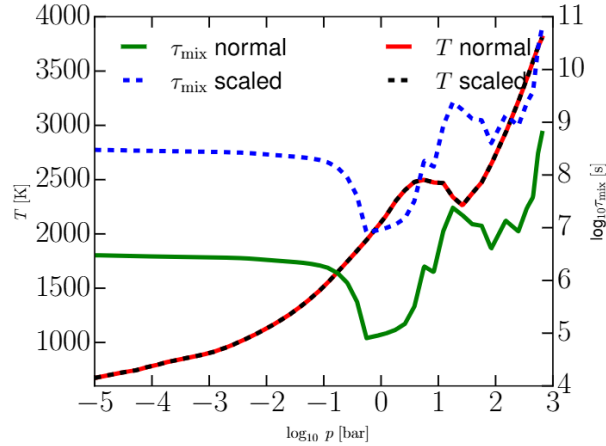


Figure 3.14: Gas temperature for more (red) and less (black) efficient mixing, mixing time scales for more (green) and less (blue) efficient mixing, created by Tamara Janz.

The gas temperature at the morning terminator shows a steady growth starting from  $10^{-5}$  bar to 10 bar. At 10 bar there is a short drop. Then the rise continues and the temperature gets higher in the deeper layers of the atmosphere. This is true for the scaled and normal mixing model as there is no difference considered.

The mixing time scale is constant for the upper layers. Before reaching 1 bar, the timescale drops to  $10^7$  s for scaled and  $10^5$  s for normal mixing. In the deeper layers, the timescale starts rising and falling again. It reaches its peak of nearly  $10^{11}$  s for scaled mixing and nearly  $10^9$  s for normal mixing in the deepest point of the atmosphere.

### Dust to gas ratio

The dust to gas ratio for the normal mixing scenario for a planet with an equilibrium temperature of 1600 K can be seen in figure 3.15. In subfigure 3.15i the planet can be seen from the equatorial slice; subfigure 3.15ii shows the terminator slice. In figure 3.16 the dust to gas ratio for scaled mixing is shown. Subfigure 3.16i is the equatorial slice and subfigure 3.16ii the terminator slice of the planet.

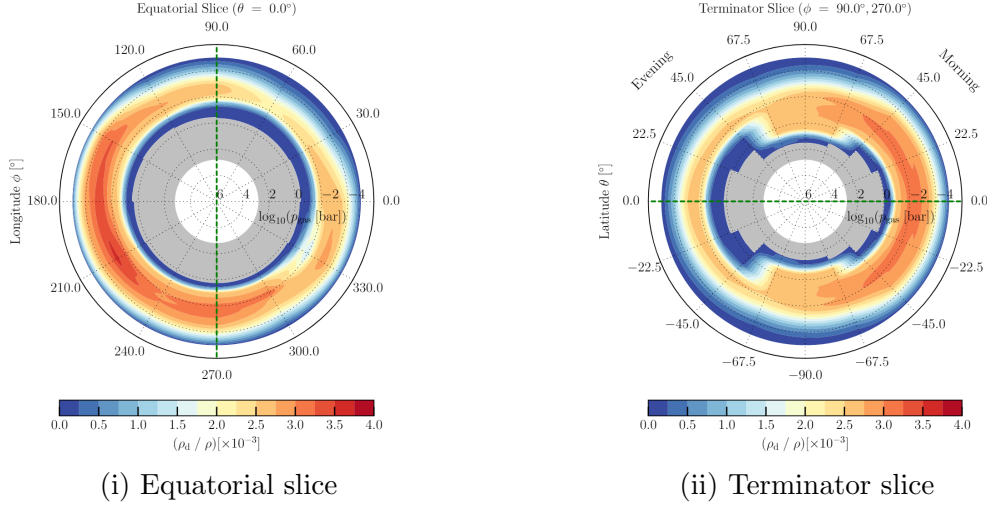


Figure 3.15: Gas to dust ratio distribution on a planet with an equilibrium temperature of 1600 K with normal mixing.

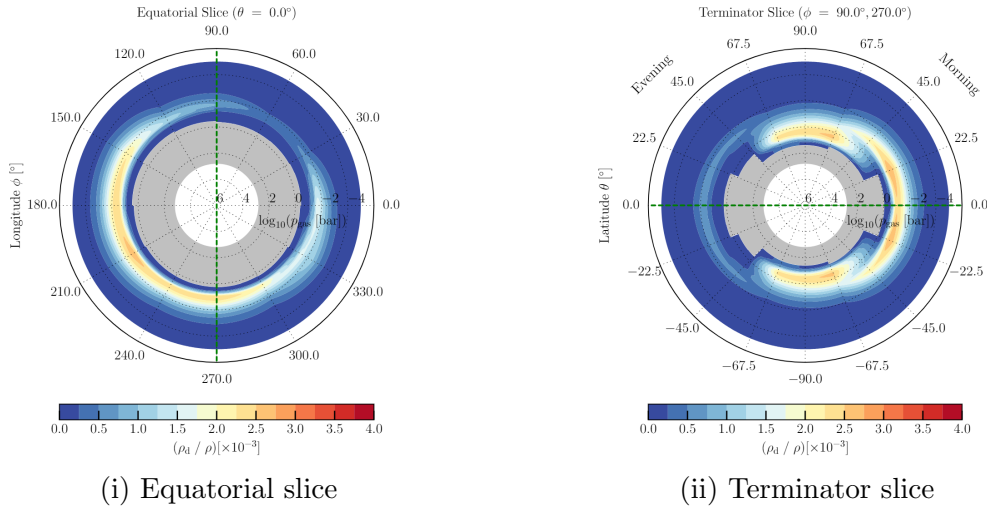


Figure 3.16: Gas to dust ratio distribution on a planet with an equilibrium temperature of 1600 K with scaled mixing.

Considering the equatorial slice, the dust to gas ratio shows that the clouds are distributed all around the planet. The night side has a higher dust to gas ratio overall and a peak of  $4 \cdot 10^{-3}$  at  $210^\circ$ . The clouds reach down to nearly 1 bar at all degrees. There is a dip in the ratio at  $60^\circ$  sinking down to  $2 \cdot 10^{-3}$  there. The majority of the clouds are between  $10^{-4}$  and  $10^{-2}$  bar, under and over that layer the ratio goes towards zero. The terminator slice shows that the morning side favour the clouds over the evening side. The clouds reach just over 1 bar down in the atmosphere. There are peaks at  $0^\circ$  on either side. The ratio is  $2 \cdot 10^{-3}$  on the evening side and  $3 \cdot 10^{-3}$  on the morning side.

For the scaled mixing model the clouds are less visible, the clouds are more developed on the night side with the peak at  $210^\circ$ . The clouds stretch from the top layer of the atmosphere down to nearly 1 bar with a higher ratio of  $3 \cdot 10^{-3}$ . There is a decrease in the clouds at  $60^\circ$  on the day side. The terminator slice shows that the clouds are at their peak on the morning side at  $22^\circ$  and  $-22^\circ$  of around  $3 \cdot 10^{-3}$ .

In picture 3.17 the dust to gas ratio at the morning terminator is depicted. Two profiles can be observed, for the normal mixing and scaled mixing model respectively.

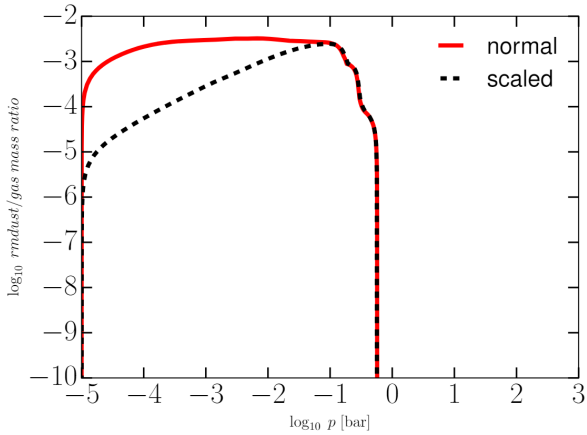


Figure 3.17: Dust to gas ratio at the morning terminator for normal (red) and scaled (black) mixing, created by Tamara Janz.

The dust to gas ratio for the normal mixing scenario begins at  $10^{-5}$  bar and is at constant value down to  $10^{-1}$  bar. At a deeper layer, the ratio starts getting smaller and goes to 0 before reaching 1 bar. The scaled mixing shows consistent growth from  $10^{-5}$  bar to  $10^{-1}$  bar. The ratio starts to get lower then and plummets towards 0 at the same point as the normal mixing profile.

### Total nucleation rate

In figure 3.18 the total nucleation rate of a planet with an equilibrium temperature of 1600 K with normal mixing is visible. Hereby, subfigure 3.18i shows the equatorial slice and 3.18ii the terminator slice. Figure 3.19 shows the scaled mixing model. In subfigure 3.19i, the planet is seen from the equatorial slice. Subfigure 3.19ii shows the terminator slice of the planet.

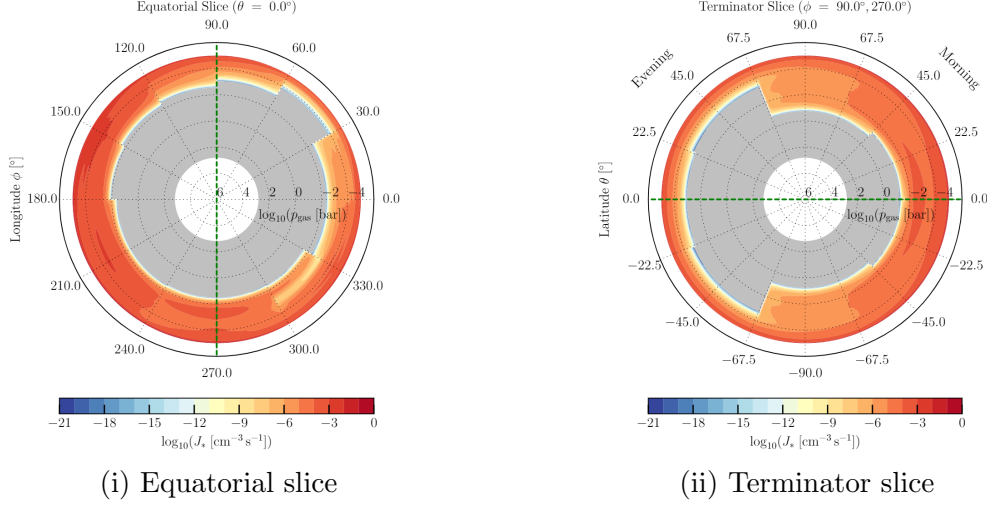


Figure 3.18: Total nucleation rate on a planet with an equilibrium temperature of 1600 K with normal mixing.

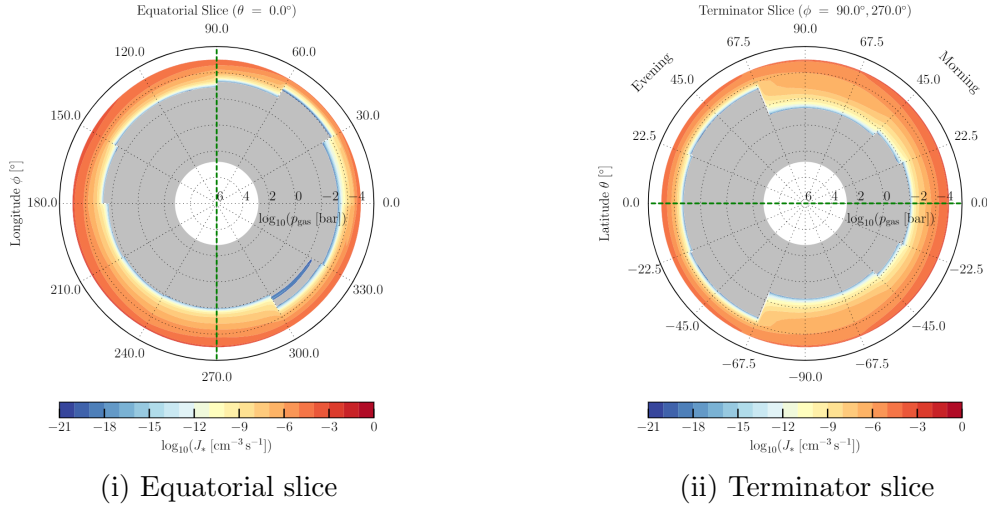


Figure 3.19: Total nucleation rate on a planet with an equilibrium temperature of 1600 K with scaled mixing.

Nucleation is possible all around the planet. Between  $180^\circ$  and  $330^\circ$  nucleation is possible down to 0.01 bar. For the area between  $30^\circ$  and  $60^\circ$  nucleation only reaches  $10^{-4}$  bar. Looking at the terminator slice nucleation happens from  $68^\circ$  on the night side and all of the morning side around to  $-68^\circ$  on the evening side. Reaching down to a layer between 0.01 bar and 1 bar there. Between  $68^\circ$  and  $-68^\circ$  nucleation reaches just over  $10^{-4}$  bar down. At the highest value, the nucleation rate reaches  $0.1 \text{ cm}^{-3}\text{s}^{-1}$ .

The total nucleation rate is less overall for the scaled mixing model. It reaches to 0.01 bar between  $180^\circ$  to  $300^\circ$ . The area from  $300^\circ$  to  $330^\circ$  has a layer over 0.01 bar where nucleation stops and reappears briefly in a deeper layer again. Between  $30^\circ$  and  $60^\circ$  nucleation reaches its minimum at  $10^{-4}$  bar. Between  $68^\circ$  on the evening side over the whole morning side to  $-68^\circ$  on the evening side, nucleation reaches to 0.01 bar and deeper. The area on the evening side spanning from  $68^\circ$  to  $-68^\circ$ , the total nucleation rate stops at just over 0.001 bar.

In figure 3.20 the total nucleation rate at the morning terminator is depicted. The profiles for the normal and scaled mixing model are visible.

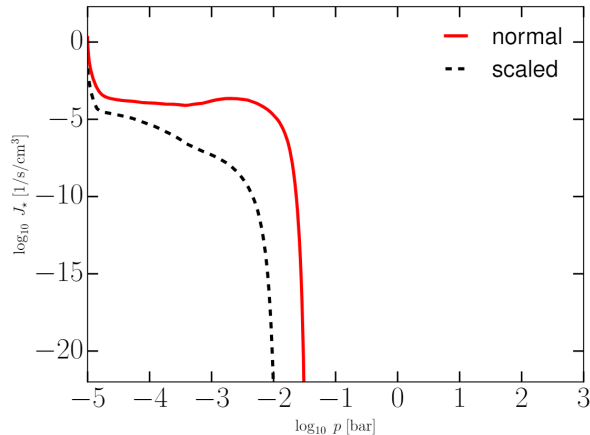


Figure 3.20: Total nucleation rate at the morning terminator for normal (red) and scaled (black) mixing, created by Tamara Janz.

Comparing the two mixing models, it is evident that the normal mixing profile reaches deeper into the atmosphere. This is because there is more material available for nucleation. It stops between  $10^{-2}$  bar and  $10^{-1}$  bar, whereas for scaled mixing it stops at  $10^{-2}$  bar. The normal mixing profile has its highest rate at  $10^{-5}$  bar, then reaching a constant value of over  $10^{-5} \text{ cm}^{-3}\text{s}^{-1}$ . At  $10^{-2}$  bar it rises shortly before plummeting to 0. For the scaled mixing, the rate is reducing the deeper the atmosphere is.

### Mean particle size

In figure 3.21, the mean particle size in the atmosphere of a planet with 1600 K equilibrium temperature and normal mixing is visible. The equatorial slice can be seen in subfigure 3.21i and the terminator slice in subfigure 3.21ii. In figure 3.22, the mean particles size for a planet with an equilibrium temperature of 1600 K and scaled mixing can be seen. In subfigure 3.22i The equatorial slice is shown; in subfigure 3.22ii the terminator slice.

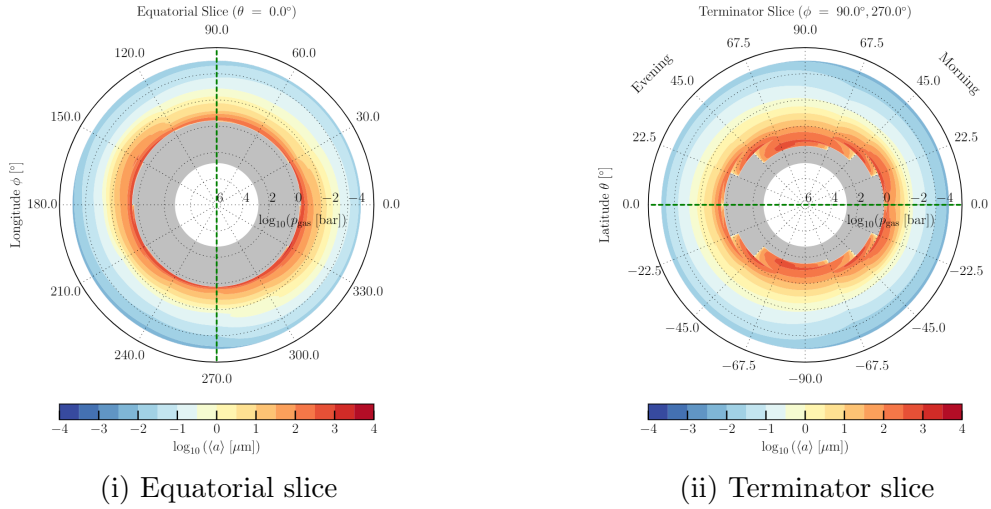


Figure 3.21: Mean particle size distribution on a planet with an equilibrium temperature of 1600 K with normal mixing.

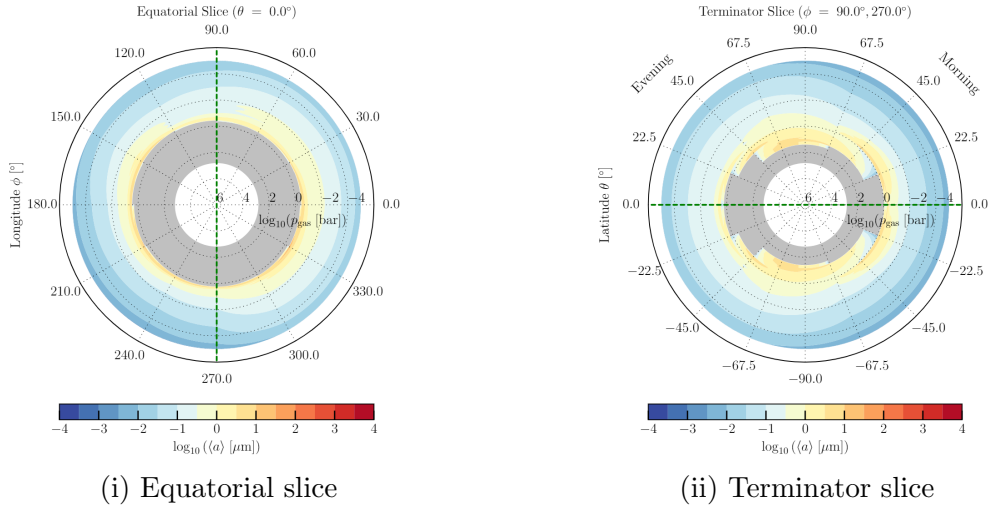


Figure 3.22: Mean particles size distribution on a planet with an equilibrium temperature of 1600 K with scaled mixing.

For the normal mixing in figure 3.21, the particles reach down into the atmosphere to nearly 1 bar. The higher the particles the smaller they are in size. At the top layer of the atmosphere the particles size is at about  $0.01 \mu\text{m}$ . Before the particles evaporate, they are at their biggest at  $1000 \mu\text{m}$ . Looking at the scenario from the terminator perspective the particles reach lower layers of the atmosphere between  $22^\circ$  and  $-22^\circ$  on the evening side and  $22^\circ$  and  $-22^\circ$  on the morning side. However, they do not differ in regard to the biggest size of the particles at the lowest point.

For the scenario with scaled mixing in figure 3.22, the particles cover an equal area as for the normal mixing model. For the scaled mixing, the particles appear to be smaller overall, reaching a size of  $1 \mu\text{m}$  to  $10 \mu\text{m}$  at their biggest. At this size the particles cease to exist before growing further. For higher latitudes in the terminator slice, the particles reach  $10 \mu\text{m}$  as their biggest size. The mean particles size is quite equally distributed, being in the atmosphere up until nearly 1 bar before they evaporate. Before evaporation they are at their biggest size.

In figure 3.23 the mean particle size at the morning terminator can be seen for normal and scaled mixing.

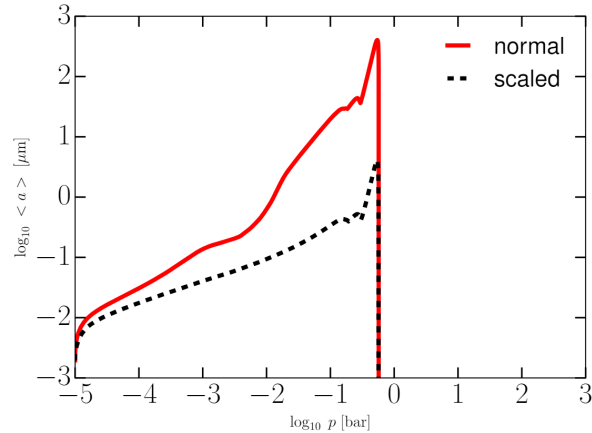


Figure 3.23: Mean particle size at the morning terminator for normal (red) and scaled (black) mixing, created by Tamara Janz.

The mean particle size is increasing the deeper it goes into the atmosphere. For normal mixing the peak happens before reaching 1 bar and the particles have a size between  $100$  and  $1000 \mu\text{m}$ . The scaled mixing profile has the peak at the same point. The size is here between  $1 \mu\text{m}$  and  $10 \mu\text{m}$ . After reaching their peak both profiles are reduced to 0.

### Number of particles

In figure 3.24 the number of particles for a planet with 1600 K equilibrium temperature at the morning terminator is depicted. The profile for normal and scaled mixing can be observed.

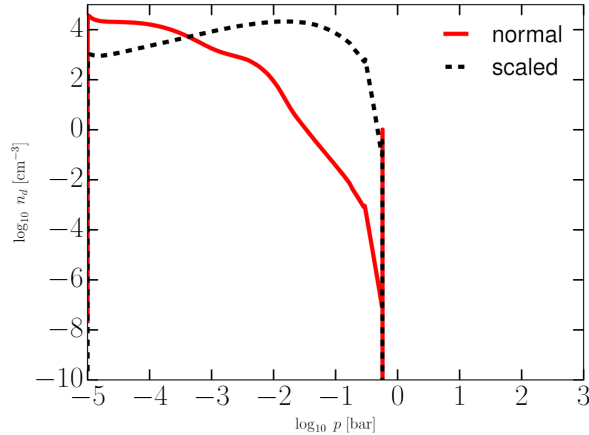


Figure 3.24: Equatorial side

Figure 3.25: Number of particles at the morning terminator for normal (red) and scaled (black) mixing, created by Tamara Janz.

At the highest layer, the normal mixing shows a higher number of particles with over  $10^4$  cm<sup>-3</sup>. Between  $10^{-3}$  and  $10^{-2}$  the scaled mixing shows a higher value in the terms of number quantity. The scaled mixing profiles keeps rising to its peak of  $10^4$  cm<sup>-3</sup>. In the area between 0.1 bar and 1 bar, it plummets to 0. The normal mixing profile is sinking throughout the atmosphere until reaching 0 at the same point.

### 3.1.3 Planets with other equilibrium temperature

Describing and discussing all simulated planets in detail would be too extended for the purpose of this bachelor thesis. An overview of the other planets can be found in the appendix 5. There, the planets with an equilibrium temperature of 2600 K down to 1200 K in 200 K steps can be found. For the scaled mixing model the 1400 K and 1200 K are not included as they were not finished in time for this thesis.

In figure 5.1 the gas temperature distribution for all simulated planets is depicted. With a smaller equilibrium temperature the gas temperature range on the planets gets smaller. For all planets the deepest layer of the atmosphere is evenly distributed and has the highest temperature there. In the higher layers the temperature is no

longer evenly distributed. It is cooler on the night side and due to the jet the cold gas gets transported over the morning terminator. There are no differences for the scaled and mixing model here.

Looking at the gas to dust ratio for normal mixing in 5.2, one can see the differences in the cloud distributions. The higher the equilibrium temperature, the less clouds exist. Furthermore, lower global temperatures enable the cloud particles to reach deeper into the atmosphere. This is because having higher temperatures means the cloud particles evaporate at an higher layer in the atmosphere and therefore cannot grow as big as they descend. The planets ranging from 1800 K to 1200 K have clouds all around the planet. The planets with higher temperatures have clouds on the night side and only partly on the day side. The planet with 1800 K has the biggest area with the highest ratio of  $4 \cdot 10^{-3}$ . The most clouds are found on the planet with 1200 K reaching down to all the considered layers of the atmosphere. The highest ratio here is  $3.2 \cdot 10^{-3}$ . The scaled mixing profiles in figure 5.3 show an equal area of the clouds distribution. Here the ratios are less and reach only  $2.75 \cdot 10^{-3}$  at most for the 1600 K planet. The peaks in the cloud ratio are in the same places as for the normal mixing, but the ratio is smaller here.

In figure 5.4 the total nucleation rates are shown for normal mixing. For 2600 K and 2400 K nucleation is possible in the upmost regions of the atmosphere. It is possible on the night side and over the morning terminator down to  $10^{-4}$  bar. For 2200 K and 2000 K, nucleation reaches even further over the morning terminator and covers even more area looking from the terminator perspective. For the remaining planets nucleation is possible all around the planet. The colder the planet, the deeper the nucleation reaches into the atmosphere. The highest nucleation rate can be found on the 2200 K planet with a rate of  $1 \text{ cm}^{-3}\text{s}^{-1}$ . For scaled mixing, nucleation is not possible as deep into the atmosphere. However, the covered areas are similar. The nucleation rate is reduced overall as well in contrast to the normal mixing models.

The mean particle size shows not only where the clouds are located in the atmosphere, but also the mean size of the individual particles. At the highest layer of the atmosphere, the particles are at their smallest. The further the particles go into the atmosphere the bigger they grow. They reach their biggest values just before the particles cease to exist as they evaporate. For normal mixing, the biggest particles are up to  $10^4 \mu\text{m}$ . The scaled mixing profile covers the same area. The particles do not reach the size of their normal mixing counterparts. The biggest size of the particles are at  $10 \mu\text{m}$  here.

## 3.2 Comparison to older models

The gas temperature for two models were compared. The profiles were observed at the sub stellar point, the anti stellar point, the morning terminator and the evening terminator. A profile for a planet with equilibrium temperatures of 2600 K is visible in figure 3.26.

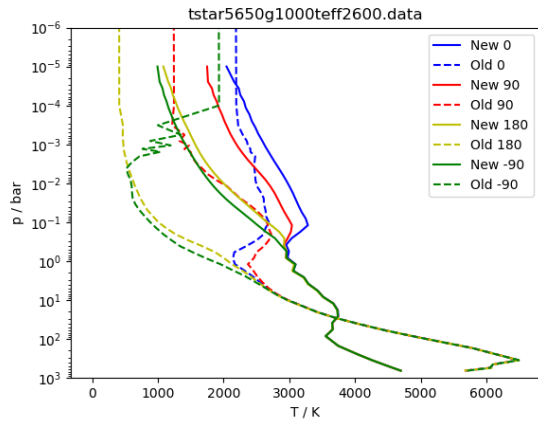


Figure 3.26: Gas temperature profiles for the old (dashed) and the new (solid) model at the sub stellar point (blue), anti stellar point (yellow), morning terminator (green) and evening terminator (red) for a planet with 2600 K equilibrium temperature.

Considering the new model, the sub stellar point is here the hottest followed by the evening terminator, the anti stellar point and the morning terminator with the coldest profile. The range in the top layer is between 900 K and 2100 K. The temperature starts rising the deeper the atmosphere. At 1 bar the profiles start converging and the temperature is evenly distributed in the lower parts of the atmosphere. The new profile reaches its maximum of 4700 K at the deepest layer of the atmosphere. For the older model, the hottest profile at the top layer is the sub stellar point then the morning terminator, the evening terminator and the anti stellar point. At  $3 \cdot 10^{-4}$  bar the morning terminator gets colder than the evening terminator. At  $3 \cdot 10^{-3}$  bar it gets even colder than the anti stellar profile. The profile starts converging at 5 bar and the profiles reach a maximum of around 6500 K. At 300 bar the temperatures get cooler again. The plots for the other equilibrium temperatures can be found in the appendix 5 in figure 5.8. For them, the lower the temperatures the smaller the distance between the individual profiles gets. The newer model has the sub stellar profile and the evening terminator intersect and change positions. The older model has its profiles intersect multiple times and has sudden falls in the temperature. For all profiles the temperatures start converging in the deeper atmosphere.

# Chapter 4

## Discussion

Looking at the gas temperature distribution in figure 3.1i, there is a shift visible. Due to the jet on the equator, the temperature gets shifted in an anticlockwise manner. The colder gas gets carried over the morning terminator due to this and the coldest part of the atmosphere is therefore not only on the night side but also over the morning terminator. Around the  $30^\circ$  part, there is an area where the temperature gets hotter again. This part would be expected on the  $0^\circ$  position as there the star has the direct impact on the planet. Due to the jet, the area gets shifted. The atmosphere getting cooler and then hotter again can be explained with the jet and the radiative transfer as this moves the hotter gas up.

Figure 3.3 shows the dust to gas ratio for normal mixing. One can see that the clouds only exist where it is cold enough meaning that the clouds mimic the positions of the colder areas, as they are able to form there. In the hotter areas the clouds start to evaporate. The scaled mixing models show less clouds as the speed of circulation is reduced and the forming process is slower. As the colder gas gets carried over the morning terminator by the jet, clouds are able to form in the lower temperatures there.

Nucleation happens in the upmost region of the atmosphere as it is cold enough there. The normal mixing having a higher nucleation rate is due to there being more particles and the mixing process being more efficient. The rate for scaled mixing is reduced, as the particles take longer to reach higher layers.

The mean particle size in figure 3.9 shows where the particles are located and how big they are. The lower the particles reach into the atmosphere, the bigger they get. Due to the bulk growth, the particles grow as they fall through the atmosphere. After reaching their biggest point, they cut off, this happens as the temperature gets too hot and the cloud particles evaporate. This is equally true for normal and scaled

mixing. After this step, the cycle starts anew. The particles grow smaller for scaled mixing as there is less material available.

Having less nucleation as in the scaled mixing could mean that therefore, the particles would be able to grow bigger. This could be explained as there are less particles to share the same mass. In the case of this simulation, this does not turn out to be true. In regard to the number of particles in figure 3.12, the scaled mixing has less in the upper atmosphere. Nucleation happens therefore less and there are less nuclei. The normal mixing has the higher value in the deeper regions meaning there are less particles that share the mass; therefore, the individual ones can grow bigger.

Having a planet with an equilibrium temperature of 1600 K means the planet is further away from its host star. The temperature overall is less in the planets atmosphere. The shift due to a jet on the equator can be observed on this planet as well.

The clouds here reach all around the planet as the temperature has low enough values all around. At 60° there is a spot where the temperature does not reach sufficient temperatures and a dip in the clouds occurs. The scaled mixing scenario shows less clouds overall. As here the particles do not get brought up as fast as for the normal mixing model.

Nucleation is more prominent for the normal mixing overall. Nucleation is possible in the higher layers as the nuclei form there and the particles start growing as they fall through the atmosphere and the clouds therefore exist under the nucleation region.

For the particle size the particles grow as they fall trough the atmosphere. As they reach their biggest point at their deepest position, they start to evaporate. The temperatures reach too high values there and the cloud particles evaporate. The circulation process of the particles is faster for the normal mixing and there are more particles to help the growth of the cloud particles. This means, for the scaled mixing the mean particle size is overall smaller here.

The number of particles in the atmosphere shows that in the upper atmosphere, there are more particles, which leads to higher rate in of nucleation. For the normal mixing, this means nucleation happens more prominently. As the particles fall through the atmosphere, the number gets less and less particles share the mass. Therefore, the individual particles can grow bigger. For the scaled mixing there are less particles available for the nucleation. In the deeper region, there are more particles sharing the mass leading to a decrease mean particles size.

Comparing all the models to the simulations in Helling et al. (2023), it is clear that the new approach with the radiative transfer has major impact. The night side for the planets does not cool as significantly as before due to the Newtonian cooling in

the old model. There are also effects for the temperature distribution all around the planet as well as the range. The clouds are therefore directly impacted as well. The nucleation is no longer possible up to equally high rates as before. It also does not reach as deep into the atmosphere and is covers a smaller area around the planet. The mean particles size and therefore the cloud distribution show differences as well. The particles are not able to grow as big and are less present on the day side. This is especially true for the scaled mixing model, as here the particles are also smaller compared to the new normal mixing model.

Comparing the two model considering the temperatures in figure 3.26, it is evident that they behave quite differently. The radiative transfer impacts not only the rate at which the temperature changes in the atmosphere but also which point is the hottest or coldest. The jet could be partly responsible for decreasing the range between the profiles for the cooler planets. As the jet is less prominent for colder and further away planets.

# Chapter 5

## Conclusion

For this thesis, cloud simulations were created for various theoretical exoplanets. Data was created that contains information about the different stages of cloud formation. This was based on a new model which included the radiative transfer happening simultaneously to the transport of material in the atmosphere. Two scenarios were considered for the mixing models. For the normal mixing, the element replenishment is an efficient process that keeps the cloud formation process active. The scaled mixing has the mixing timescale reduced by the factor 100. Here, the process is not as efficient and it leads to less clouds in the atmosphere. Planets for each models were simulated with equilibrium temperatures of 2600 K to 1200 K in 200 K steps. At the point of writing this thesis, the 1400 K and 1200 K were not yet finished for the scaled mixing which is why they are excluded here. For all planets, the data containing the nucleation process, the bulk growth and eventually the clouds' locations, have been created. There is also information on the number of particles and their elemental composition. This data, in an attempt to be more attainable, has been visualised with plots showcasing different parameters. This thesis gives an overview of the cloud formation process on tidally locked hot Jupiters which are orbiting a G-type host star.

For future projects, the clouds could be put directly into the General Circulation Model. This would consider the impact of the clouds on the temperature in the planet's atmosphere. What is more, planets with a lower equilibrium temperature than 1200 K could be simulated. To get a more accurate picture of the planet's atmosphere, choosing a finer grid could be considered as well. The cloud simulations with the new model could also be made for M and K stars like it has been done in Helling et al. (2023). To come to an end, there are certainly many more options and possibilities for future projects that could lead to a deeper understanding about the cloud formation in exoplanetary atmospheres.

# Bibliography

- R. Baeyens, L. Decin, L. Carone, O. Venot, M. Agúndez, and P. Mollière. Grid of pseudo-2D chemistry models for tidally locked exoplanets - I. The role of vertical and horizontal mixing. *MNRAS*, 505(4):5603–5653, Aug. 2021. doi: 10.1093/mnras/stab1310.
- R. Baeyens, T. Konings, O. Venot, L. Carone, and L. Decin. Grid of pseudo-2D chemistry models for tidally locked exoplanets - II. The role of photochemistry. *MNRAS*, 512(4):4877–4892, June 2022. doi: 10.1093/mnras/stac809.
- L. Carone, R. Baeyens, P. Mollière, P. Barth, A. Vazan, L. Decin, P. Sarkis, O. Venot, and T. Henning. Equatorial retrograde flow in WASP-43b elicited by deep wind jets? *MNRAS*, 496(3):3582–3614, Aug. 2020. doi: 10.1093/mnras/staa1733.
- C. Helling. Exoplanet Clouds. *Annual Review of Earth and Planetary Sciences*, 47: 583–606, May 2019. doi: 10.1146/annurev-earth-053018-060401.
- C. Helling. Clouds in Exoplanetary Atmospheres. In N. Madhusudhan, editor, *ExoFrontiers; Big Questions in Exoplanetary Science*, pages 20–1. 2021. doi: 10.1088/2514-3433/abfa8fch20.
- C. Helling. Cloud formation in Exoplanetary Atmospheres. *arXiv e-prints*, art. arXiv:2205.00454, May 2022. doi: 10.48550/arXiv.2205.00454.
- C. Helling, R. Klein, P. Woitke, U. Nowak, and E. Sedlmayr. Dust in brown dwarfs. IV. Dust formation and driven turbulence on mesoscopic scales. *A&A*, 423:657–675, Aug. 2004. doi: 10.1051/0004-6361:20034514.
- C. Helling, P. Woitke, and W. F. Thi. Dust in brown dwarfs and extra-solar planets. I. Chemical composition and spectral appearance of quasi-static cloud layers. *A&A*, 485(2):547–560, July 2008. doi: 10.1051/0004-6361:20078220.
- C. Helling, D. Samra, D. Lewis, R. Calder, G. Hirst, P. Woitke, R. Baeyens, L. Carone, O. Herbort, and K. L. Chubb. Exoplanet weather and climate regimes with clouds

- 
- and thermal ionospheres. A model grid study in support of large-scale observational campaigns. *A&A*, 671:A122, Mar. 2023. doi: 10.1051/0004-6361/202243956.
- D. D. B. Koll. A Scaling for Atmospheric Heat Redistribution on Tidally Locked Rocky Planets. *ApJ*, 924(2):134, Jan. 2022. doi: 10.3847/1538-4357/ac3b48.
- D. Samra, C. Helling, K. L. Chubb, M. Min, L. Carone, and A. D. Schneider. Clouds form on the hot Saturn JWST ERO target WASP-96b. *A&A*, 669:A142, Jan. 2023. doi: 10.1051/0004-6361/202244939.
- A. D. Schneider, L. Carone, L. Decin, U. G. Jørgensen, P. Mollière, R. Baeyens, S. Kiefer, and C. Helling. Exploring the deep atmospheres of HD 209458b and WASP-43b using a non-gray general circulation model. *A&A*, 664:A56, Aug. 2022. doi: 10.1051/0004-6361/202142728.
- P. Woitke and C. Helling. Dust in brown dwarfs. II. The coupled problem of dust formation and sedimentation. *A&A*, 399:297–313, Feb. 2003. doi: 10.1051/0004-6361:20021734.
- P. Woitke and C. Helling. Dust in brown dwarfs. III. Formation and structure of quasi-static cloud layers. *A&A*, 414:335–350, Jan. 2004. doi: 10.1051/0004-6361:20031605.

# Appendix

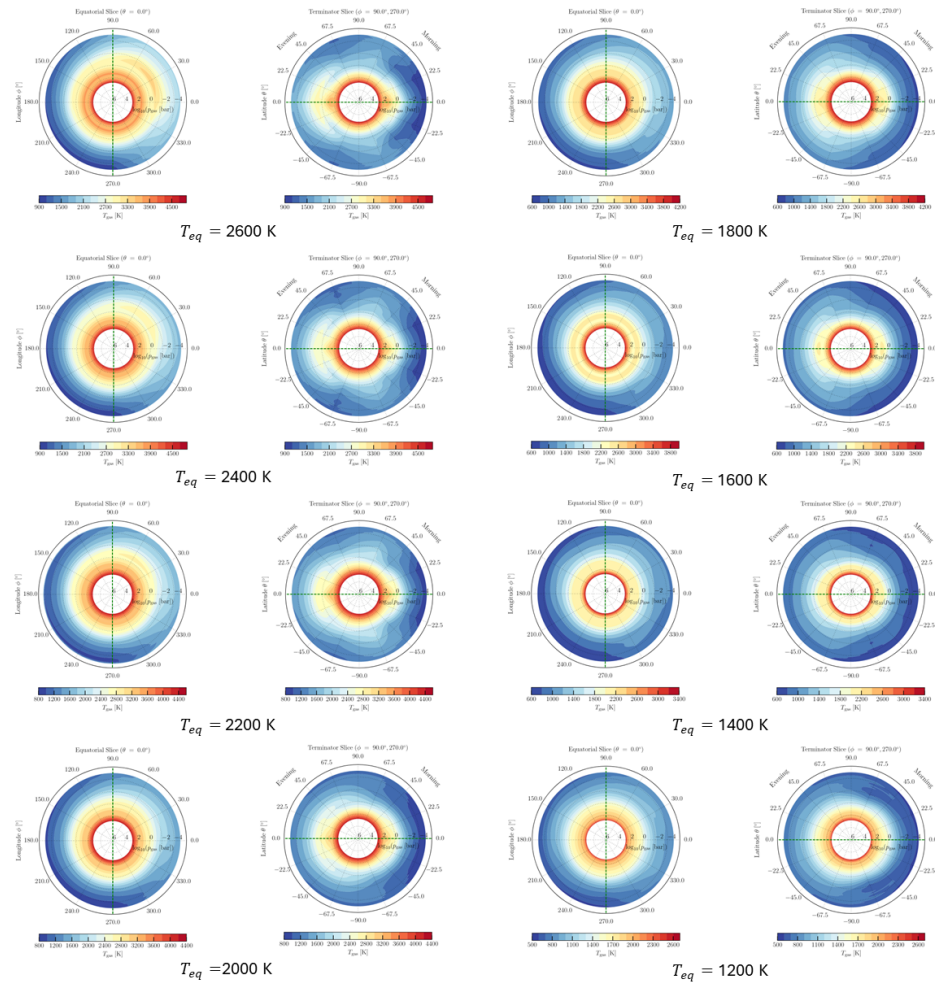


Figure 5.1: Gas temperature distribution for planets with equilibrium temperatures of 2600 K, 2400 K, 2200 K, 2000 K, 1800 K, 1600 K, 1400 K, 1200 K seen from the terminator and equatorial slices.

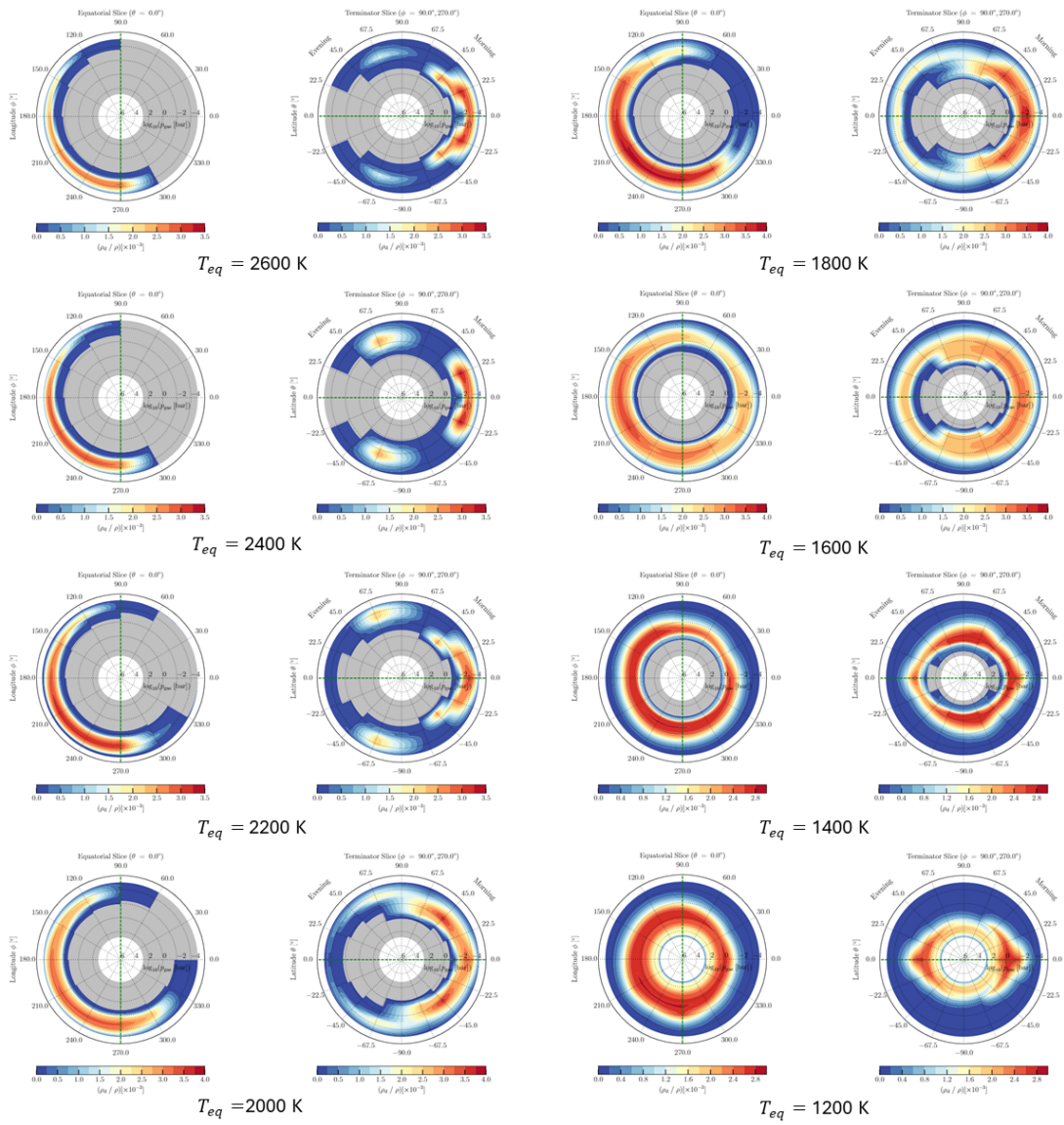


Figure 5.2: Dust to gas ratio with normal mixing for planets with equilibrium temperatures of 2600 K, 2400 K, 2200 K, 2000 K, 1800 K, 1600 K, 1400 K, 1200 K seen from the terminator and equatorial slices.

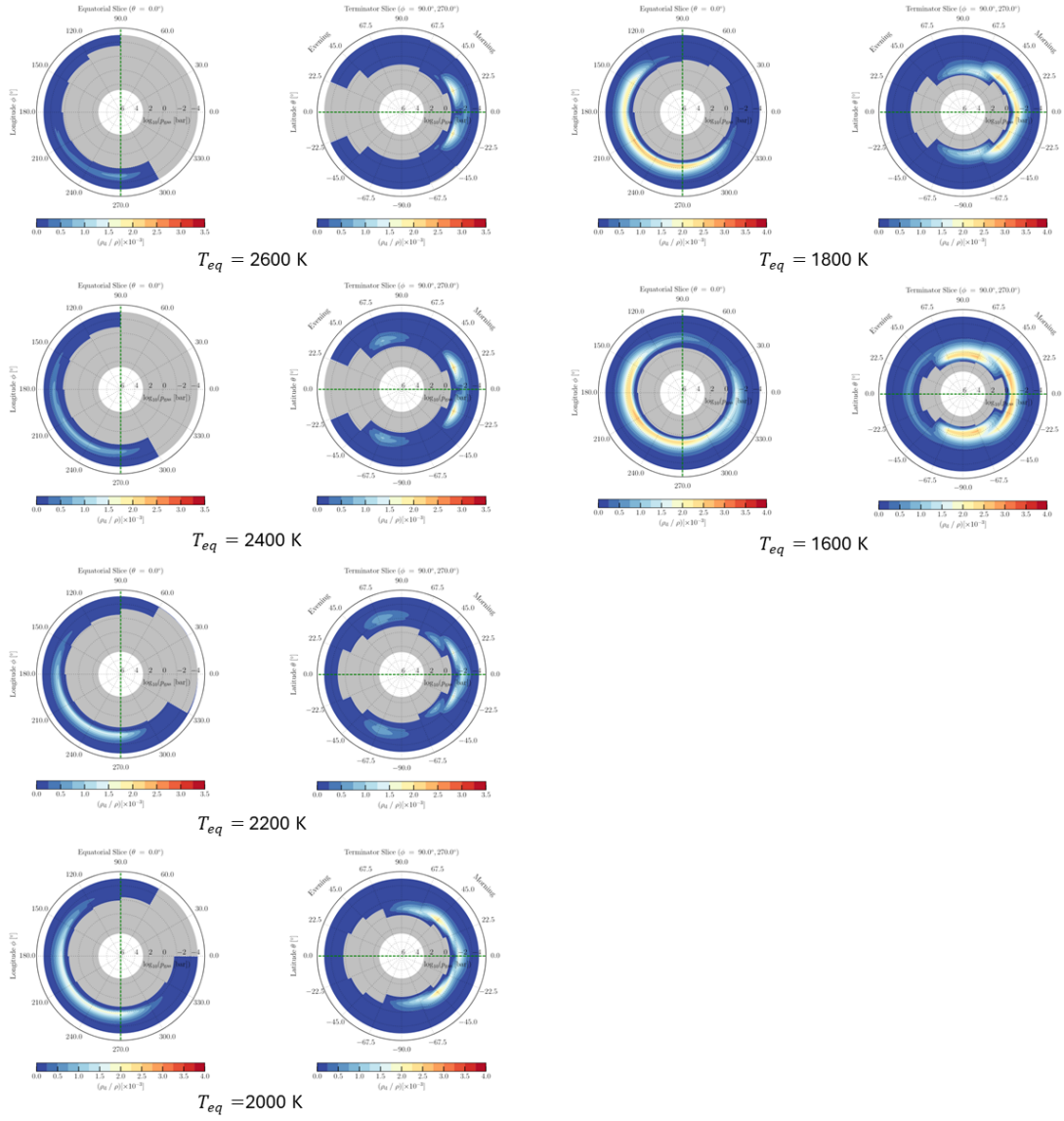


Figure 5.3: Dust to gas ratio with scaled mixing for planets with equilibrium temperatures of 2600 K, 2400 K, 2200 K, 2000 K, 1800 K, 1600 K seen from the terminator and equatorial slices.

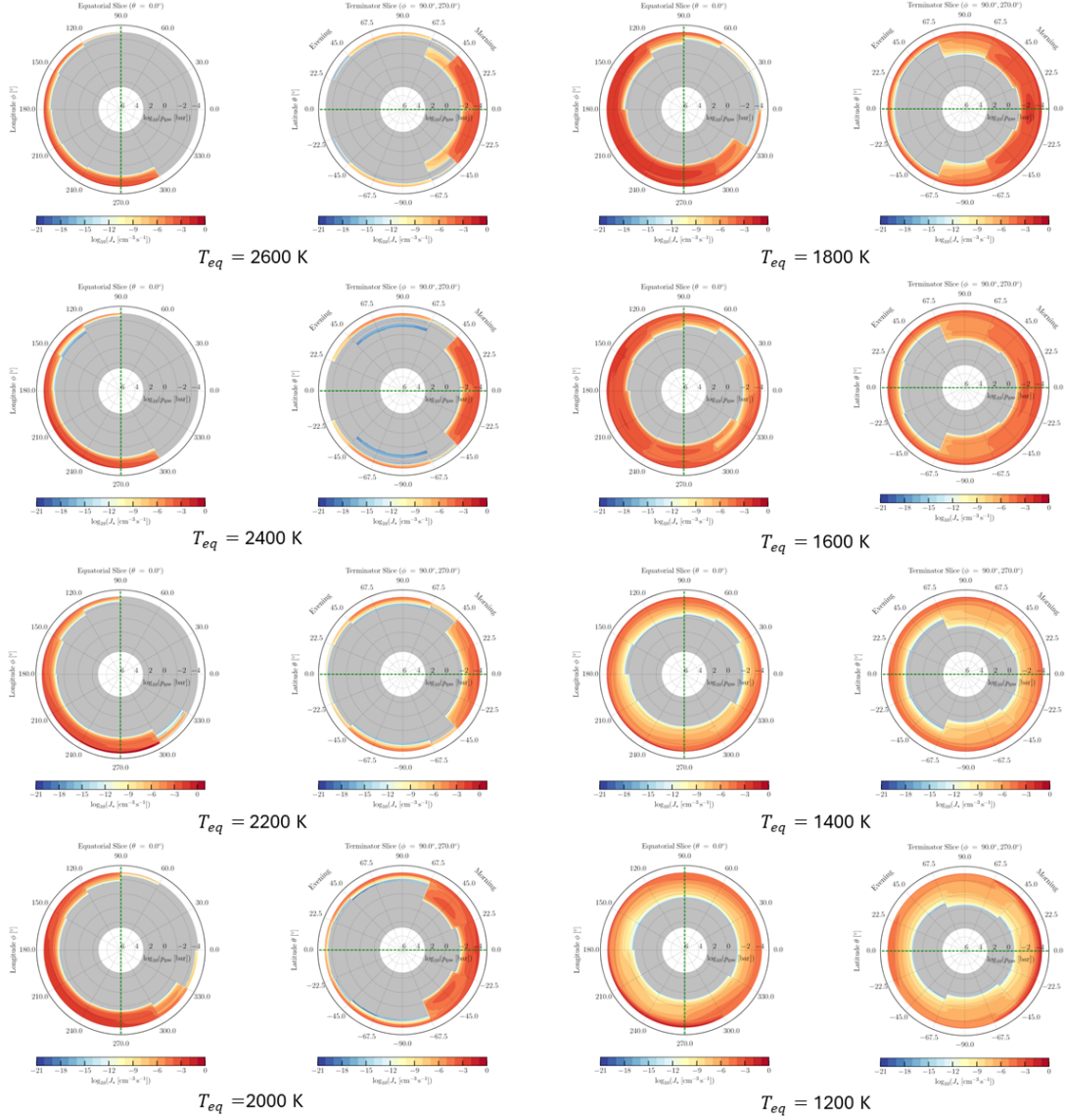


Figure 5.4: Total nucleation rate with normal mixing for planets with equilibrium temperatures of 2600 K, 2400 K, 2200 K, 2000 K, 1800 K, 1600 K, 1400 K, 1200 K seen from the terminator and equatorial slices.

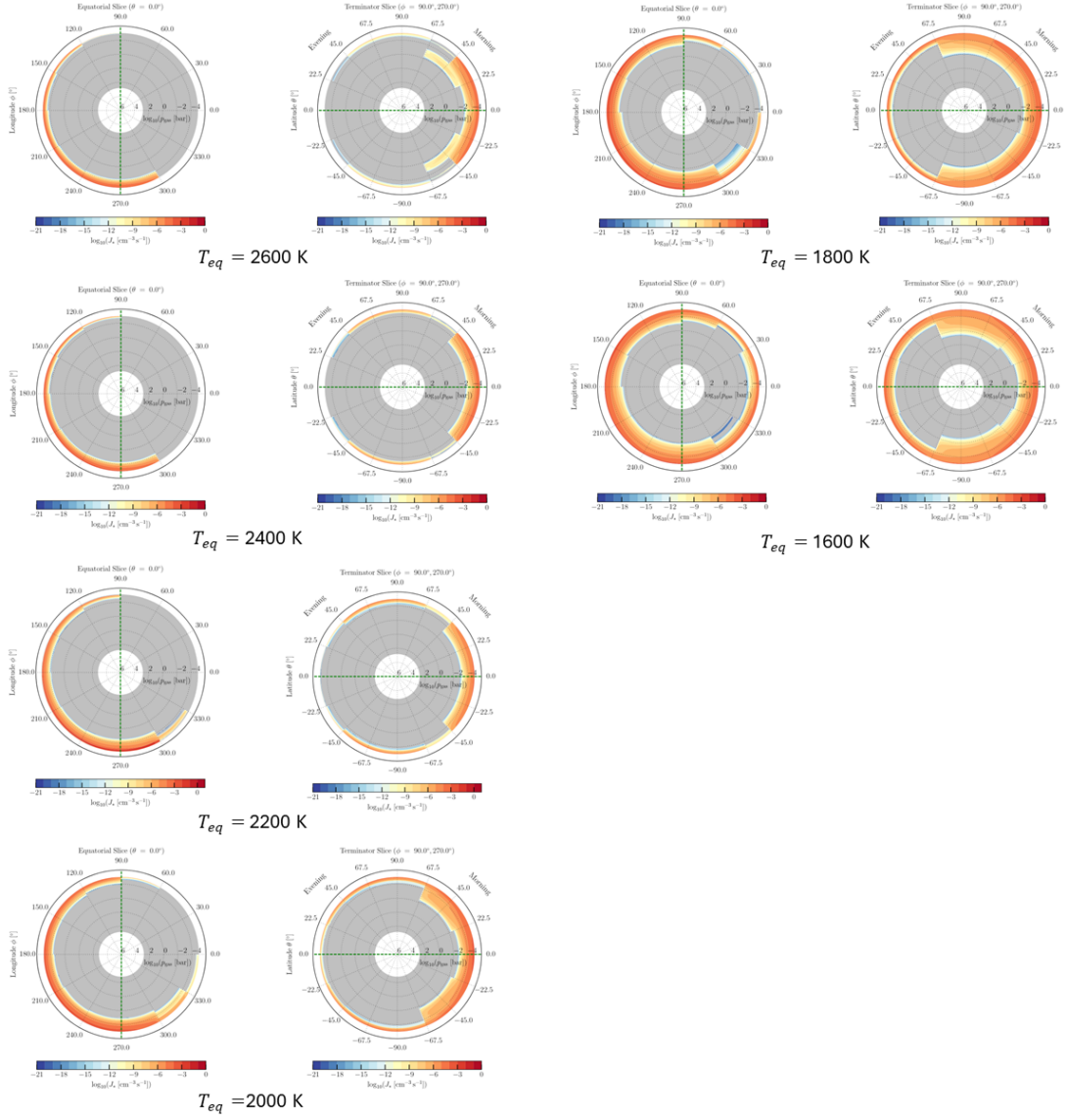


Figure 5.5: Total nucleation rate with scaled mixing for planets with equilibrium temperatures of 2600 K, 2400 K, 2200 K, 2000 K, 1800 K, 1600 K seen from the terminator and equatorial slices.

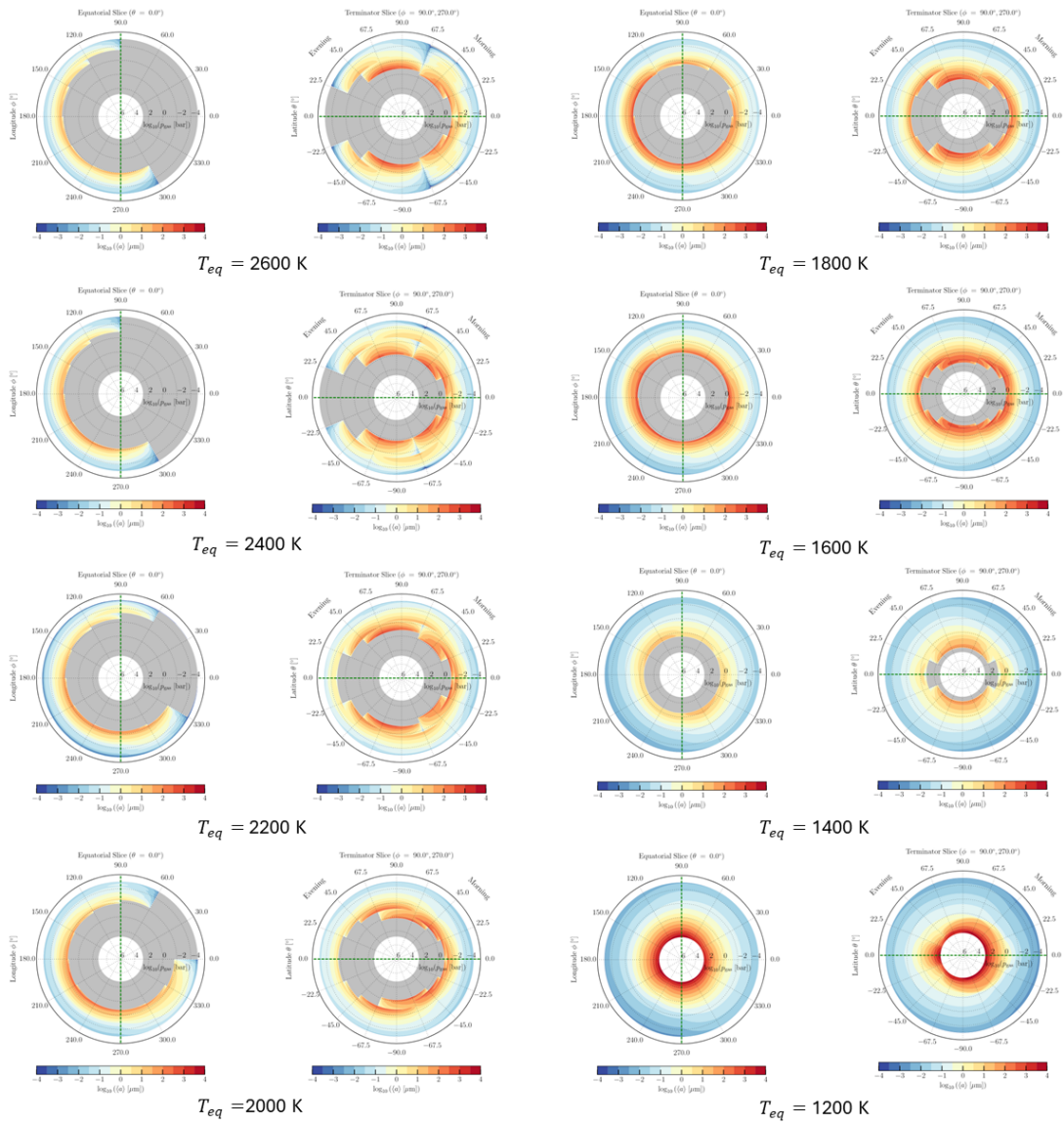


Figure 5.6: Mean particle size with normal mixing for planets with equilibrium temperatures of 2600 K, 2400 K, 2200 K, 2000 K, 1800 K, 1600 K, 1400 K, 1200 K seen from the terminator and equatorial slices.

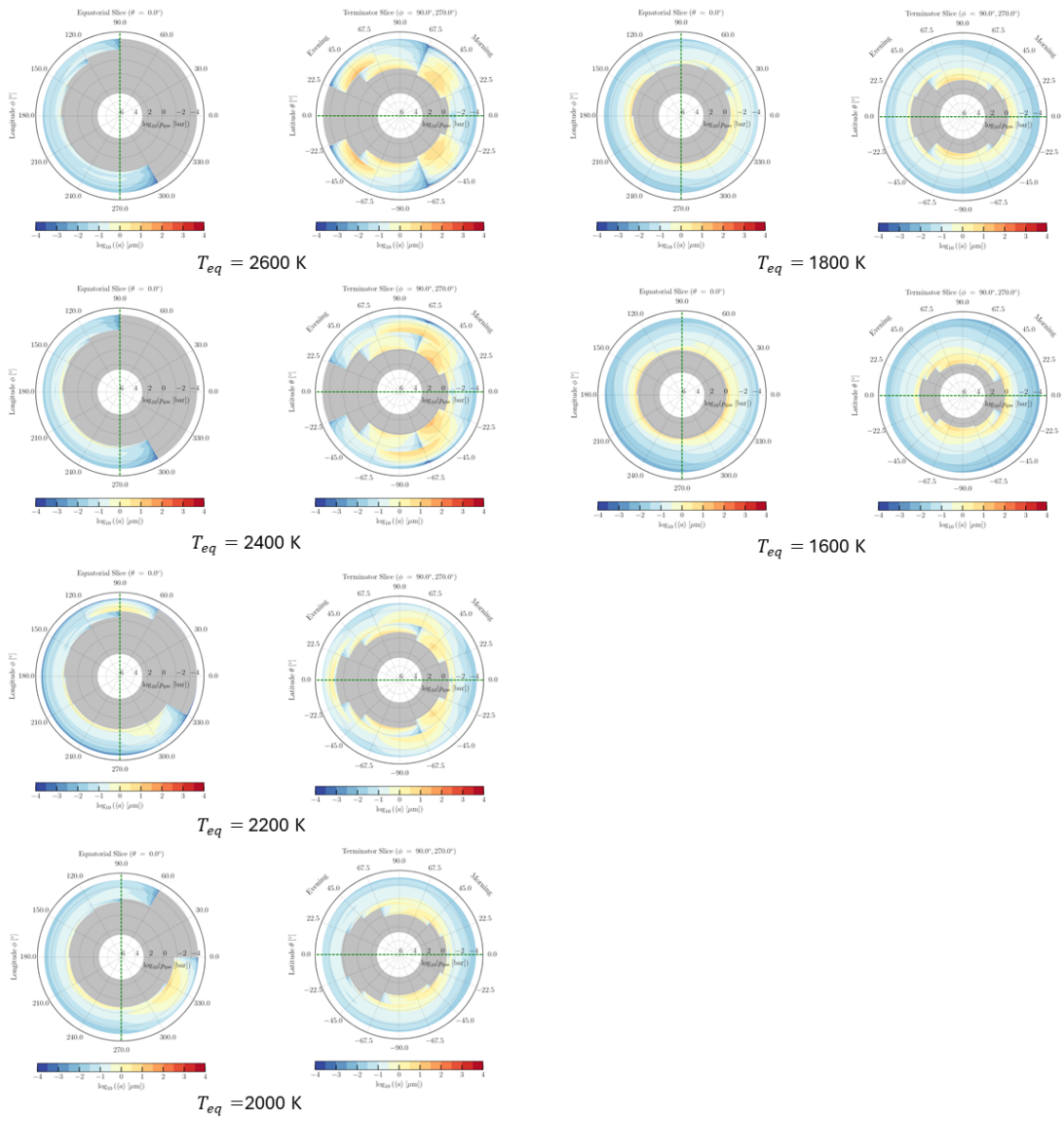


Figure 5.7: Mean particles size with scaled mixing for planets with equilibrium temperatures of 2600 K, 2400 K, 2200 K, 2000 K, 1800 K, 1600 K seen from the terminator and equatorial slices.

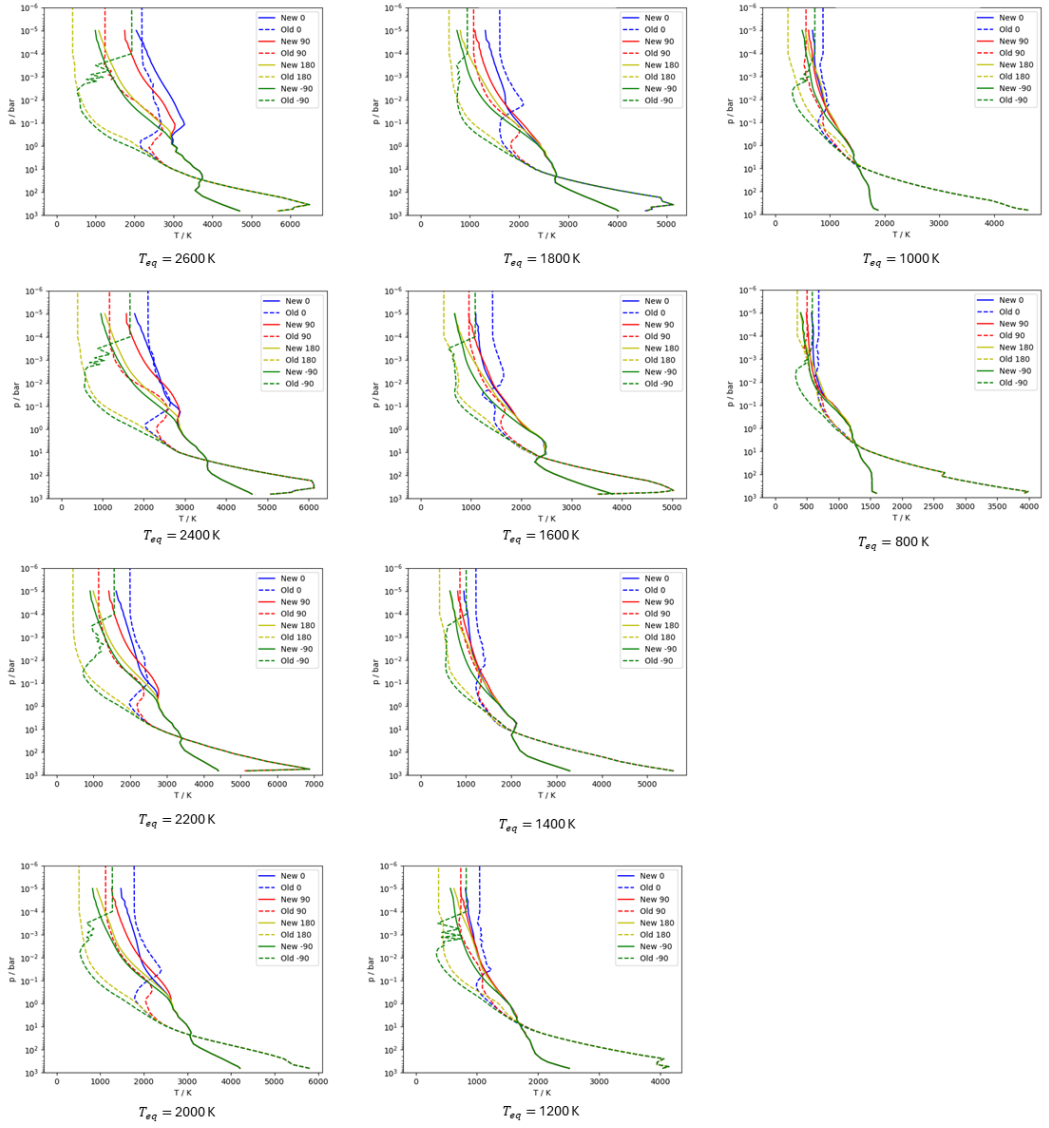


Figure 5.8: Comparison plots for the gas temperature for the old and new model for equilibrium temperatures of 2600 K, 2400 K, 2200 K, 2000 K, 1800 K, 1600 K, 1400 K, 1200 K, 1000 K, 800 K.